

Advance Publication Cover Page



**Ultrafast Dynamics in Nonaromatic Cation Based Ionic Liquids:  
A Femtosecond Raman-Induced Kerr Effect Spectroscopic Study**

Hideaki Shirota,\* Masatoshi Ando, Shohei Kakinuma, and Kotaro Takahashi

Advance Publication on the web July 28, 2020

doi:10.1246/bcsj.20200198

© 2020 The Chemical Society of Japan

Advance Publication is a service for online publication of manuscripts prior to releasing fully edited, printed versions. Entire manuscripts and a portion of the graphical abstract can be released on the web as soon as the submission is accepted. Note that the Chemical Society of Japan bears no responsibility for issues resulting from the use of information taken from unedited, Advance Publication manuscripts.

# Ultrafast Dynamics in Nonaromatic Cation Based Ionic Liquids:

## A Femtosecond Raman-Induced Kerr Effect Spectroscopic Study

Hideaki Shirota,\* Masatoshi Ando, Shohei Kakinuma, and Kotaro Takahashi

Department of Chemistry, Chiba University, 1-33 Yayoi, Inage-ku, Chiba 263-8522

E-mail: shirota@faculty.chiba-u.jp

### Abstract

Herein, the data of the intermolecular vibrations of forty nonaromatic cation based ionic liquids (ILs) at 293 K measured by femtosecond Raman-induced Kerr effect spectroscopy are reported. The low-frequency spectra in the frequency range of 0.3–700  $\text{cm}^{-1}$  were obtained by Fourier transform deconvolution analysis. The line shape of the low-frequency spectra below  $\sim 200 \text{ cm}^{-1}$  were discussed on the basis of the ion species. The spectral intensity in nonaromatic cation based ILs was much lower than that in aromatic cation based ILs owing to the absence of the aromatic ring, i.e., the libration of the aromatic species had a strong spectral intensity in the low-frequency region. However, nonaromatic cation based ILs with a flat anion, such as dicyanamide and tricyanomethide, showed stronger spectral intensity because of the libration of the anion. Other unique spectral features were also discussed in the context of the structure of the ion species. Liquid properties, such as density, viscosity, electrical conductivity, and surface tension, were also estimated. On comparing the low-frequency spectra with the bulk liquid properties of the nonaromatic cation based ILs, a mild linear relationship between the first moment of the low-frequency spectra and a bulk parameter comprised of surface tension and density was observed.

**Keywords:** Nonaromatic Cation Based Ionic Liquids, Low-Frequency Spectrum, femtosecond Raman Induced Kerr Effect Spectroscopy

### 1. Introduction

Intermolecular vibrational dynamics in liquids and solutions is a central theme in chemistry, physics, and biology, because it significantly influences the elementary processes of chemical reactions such as electron transfer, proton transfer, and isomerization in solutions, the dynamics of structural changes in biological systems, phase transition dynamics, and so on.<sup>1,2</sup> Fortunately, the development of femtosecond laser technology has made it possible to detect the time-domain data of intermolecular vibrations in liquids and solutions directly.

Intermolecular vibrations, such as libration, collision- and interaction-induced motions, in liquids and solutions occur on the time scale ranging from subpicoseconds to picoseconds, which corresponds to the terahertz region in the frequency domain. Femtosecond Raman-induced Kerr effect spectroscopy (fs-RIKES) and time-domain terahertz spectroscopy (THz-TDS) are especially suited for obtaining low-frequency (or terahertz) spectra.<sup>3-6</sup> The former technique captures the polarizability response and the latter one observes the dipole response. Further, these time-domain spectroscopic techniques provide low-frequency spectra with a high signal to noise ratio and in lower-frequency range in comparison with conventional

frequency domain spectroscopies, such as steady-state Raman and far-infrared (far-IR) spectroscopies. In particular, fs-RIKES can even be used to observe orientational dynamics in liquids and solutions. By virtue of these advantageous attributes, fs-RIKES has often been used to study the intermolecular vibrational and orientational dynamics in liquids and solutions,<sup>7-13</sup> as well as complex systems.<sup>14-16</sup>

Ionic liquids (ILs), the target material in this study, are molten salts at room temperature.<sup>17,18</sup> They exhibit unique properties, such as a low melting point (for salts), non-volatility at ambient temperature and pressure conditions (for liquids), high electrical conductivity, viscous behavior, glass-forming nature, inhomogeneous structure, and so on.<sup>19,20</sup> The molecular and reaction dynamics and photochemistry in ILs often shows characteristic behavior in comparison with common (neutral) solvents.<sup>21-25</sup> The unique features in ILs are mainly attributed to the amphiphilic nature of the cation in most cases, which forms complicated microscopic structures and engages in intermolecular interactions.<sup>26-29</sup> Accordingly, it is important to study the intermolecular vibrations in ILs to understand the molecular-level aspects of ILs, because the intermolecular vibration directly reflects on the microscopic structure and intermolecular interactions. To date, the intermolecular vibrations in ILs have been studied by time- and frequency-domain Raman and IR spectroscopies.<sup>30-36</sup> In particular, fs-RIKES has been extensively used to study ILs,<sup>37-45</sup> IL mixtures,<sup>46-55</sup> and IL-related deep eutectic solvents,<sup>56</sup> because the detection frequency range of fs-RIKES (approximately 0.3–700  $\text{cm}^{-1}$  in our setup) is sufficiently wide in the frequency range for studying the intermolecular vibrations of liquids, except for water.<sup>57,58</sup> However, as previous studies focus on specific and topical themes, a systematic overview of the intermolecular vibrations of ILs based on a large number of samples is still needed.

In 2016, we have reported the spectral data of the intermolecular vibrational dynamics of forty aromatic cation based ILs, such as imidazolium- and pyridinium-based ILs, gathered using fs-RIKES.<sup>59</sup> The unique features of the low-frequency Kerr spectra of aromatic cation based ILs were discussed based on the constituent ion species. Furthermore, a linear relation between the first moment ( $M_1$ ) of the low-frequency spectrum and the bulk parameter (square root of surface tension divided by density,  $(\gamma/\rho)^{1/2}$ ) was discovered.

This study is a continuation of our previous work.<sup>59</sup> The intermolecular vibrational dynamics of forty nonaromatic cation based ILs was investigated by fs-RIKES. The majority of published reports on the intermolecular vibrations of ILs study aromatic cation based ILs, and the number of the reports on nonaromatic cation based ILs is rather limited.<sup>41,44,45,60-66</sup> Therefore, the main objectives in this study are: (i) collecting the intermolecular vibrational spectrum data of a substantial

number of nonaromatic cation based ILs, (ii) overviewing and elucidating the unique spectral features of such ILs, and (iii) examining the relationship between the intermolecular vibrations and bulk properties. The data relating to the liquid properties of the forty nonaromatic cation based ILs, such as density  $\rho$ , viscosity  $\eta$ , electrical conductivity  $\sigma$ , and surface tension  $\gamma$ , are also reported in this study.

## 2. Experiments and Quantum Chemistry Calculations

While most ILs used in this study were obtained from chemical companies, several ILs were synthesized<sup>60,61,63,67</sup> according to the protocols established in our laboratory.<sup>61,68-70</sup> The sample ILs studied here and their abbreviations, as well as their sources, are listed in Table 1. Since the cation in [N<sub>112Bz</sub>][NTf<sub>2</sub>] has an aromatic ring, the IL might not be very suitable to treat as a “nonaromatic” cation based IL. But, we tentatively categorize [N<sub>112Bz</sub>][NTf<sub>2</sub>] into nonaromatic cation based IL in this study. This is because; the cation is an ammonium cation whose charged moiety is not aromatic, and the plot of  $M_1$  vs.  $(\gamma/\rho)^{1/2}$  for 1-benzyl-1-methylpyrrolidinium bis(trifluoromethylsulfonyl)amide showed the relation for nonaromatic cation based ILs, not for aromatic cation based ILs.<sup>44</sup> [Pyr<sub>113</sub>][DCA] obtained from Iolitec was slightly yellow in color, and was therefore purified by activated charcoal treatment using acetonitrile as a solvent to be colorless. The synthesized ILs were characterized by <sup>1</sup>H NMR and elementary analysis (SI2-1 of the Electronic Supporting Information). In elementary analysis, the obtained values of carbon, hydrogen, and nitrogen for the ILs agreed with their calculated values within  $\pm 0.4\%$ . The details of the preparation methods and analytical data of the synthesized ILs are summarized in the Electronic Supporting Information (SI2-1). The sample ILs were dried in a vacuum oven at 313 K for more than 36 h before experiments.

The densities ( $\rho$ ) of the ILs were measured at  $293.0 \pm 0.2$  K with a densitometer (Anton Paar, DMA 4100 M). The viscosities ( $\eta$ ) of the ILs were determined using a reciprocating electromagnetic piston viscometer (Cambridge Viscosity, ViscoLab 4100) equipped with a circulating water bath (Yamato, BB300) at  $293.0 \pm 0.2$  K. The electrical conductivities ( $\sigma$ ) of the samples were measured by an electrical conductivity meter (Mettler Toledo, S470 SevenExcellence) kept at  $293.0 \pm 0.2$  K using a laboratory assembled Peltier module temperature controller (VICS, VPE35-5-20TS). The surface tensions ( $\gamma$ ) of the samples were obtained using a contact angle meter (Kyowa Interface Science, DMS-401) maintained at  $293.0 \pm 0.2$  K by a circulating water bath (EYELA, NBC-1210). When the measured values of the liquid properties of the ILs differed significantly from the reported values, the measurements were repeated to confirm the obtained data. The water contents of the sample ILs were estimated by Karl Fischer titrations using a coulometer (Hiranuma, AQ-300). The water content values of the ILs are summarized in Table 2 (vide infra).

The details of the femtosecond optical heterodyne detected (OHD) RIKES apparatus built in our laboratory have been reported previously.<sup>13,71</sup> In the current fs-OHD-RIKES setup, the light source was a titanium sapphire laser (KMLabs, Griffin) pumped by the second harmonic light of a Nd:YVO<sub>4</sub> diode laser (Spectra Physics, Millennia Pro 5sJ).<sup>72</sup> The output power of the titanium sapphire laser was approximately 420 mW. The temporal response of the fs-RIKES setup was measured using a 200  $\mu$ m thick KDP crystal (type I) as the cross-correlation between the pump and probe pulses, and it was typically approximately 38 fs (full-width at half-maximum, FWHM). In the fs-RIKES experiments, scans with a high time

resolution of 3072 points at 0.5  $\mu$ m/step that corresponds to 3.34 fs/step) were made for a short time window ( $\sim 10.2$  ps). Measurements of longer time window transients ( $\sim 334$  ps) of 2000 points at 25.0  $\mu$ m/step that corresponds to 167 fs/step were also made. A pure heterodyne signal was obtained by recording the scans for both plus and minus  $\sim 1.5^\circ$  rotations of the input probe beam using a quarter wave plate; these signals were then combined to eliminate the residual homodyne signal. The rotations of the probe beam polarization using the quarter wave plate were performed while monitoring the intensity of the local oscillator. The numbers of scans for the short and long time window transients were 3 and 5 in each polarization, respectively. The ILs were injected into a 3 mm optical path length quartz cell (Tosoh Quartz) through either a 0.2  $\mu$ m or 0.02  $\mu$ m pore size Anotop filter (Whatman). During the fs-RIKES experiments, the samples were kept at a temperature of  $293.0 \pm 0.2$  K by a Peltier-based temperature controller (Quantum Northwest, Luma 40).

Density functional theory (DFT) quantum chemistry calculations based on the B3LYP/6-311+G(d,p) level of theory<sup>73,74</sup> were performed for geometry optimizations of some cations and anions using the Gaussian 16 program.<sup>75</sup> Normal mode Raman spectra of some cations and anions were calculated on the basis of their optimized structures. Using the polarizability tensor elements  $\alpha_{ij}$  of optimized ions, the mean polarizability  $\alpha_0$  was calculated using eq. (1)<sup>76</sup>

$$\alpha_0 = \frac{\alpha_{xx} + \alpha_{yy} + \alpha_{zz}}{3} \quad (1)$$

and the polarizability anisotropy  $\alpha_{anis}$  was calculated by,<sup>76</sup>

$$\alpha_{anis} = \left\{ \left[ (\alpha_{xx} - \alpha_{yy})^2 + (\alpha_{yy} - \alpha_{zz})^2 + (\alpha_{zz} - \alpha_{xx})^2 + 6(\alpha_{xy}^2 + \alpha_{yz}^2 + \alpha_{zx}^2) \right] / 2 \right\}^{1/2} \quad (2)$$

The atom coordinates of the optimized geometries of cations and anions are summarized in Tables S2-3 and S2-4 of the Electronic Supporting Information.

## 3. Data Analysis

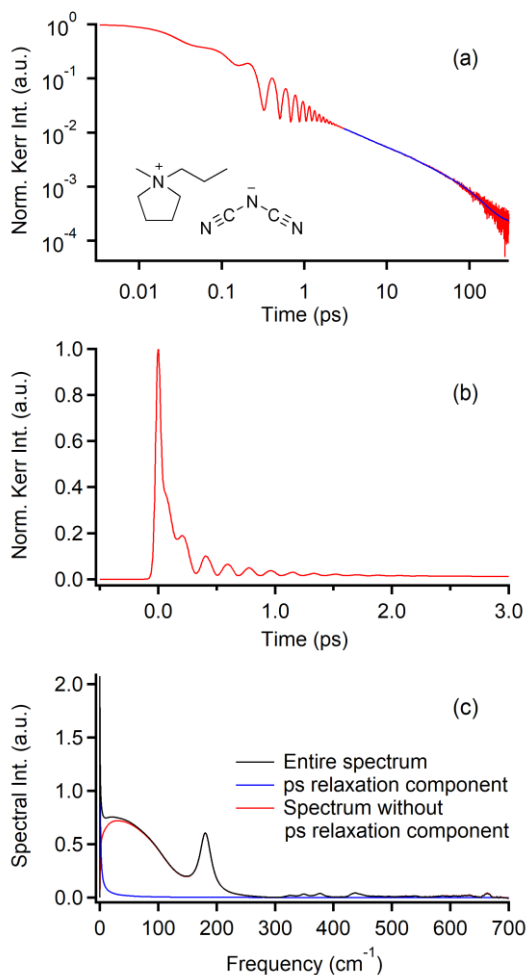
The time-domain data (Kerr transients) of the ILs measured with fs-RIKES were analyzed on the basis of the standard Fourier transform deconvolution analysis method developed by McMorro and Lotshaw<sup>77,78</sup> to obtain the low-frequency spectra. The details of the Fourier transform deconvolution analysis procedure followed in our laboratory has already been reported elsewhere.<sup>13,34</sup> In this study, the analytical method was exactly the same as in our previous report on forty aromatic cation based ILs,<sup>59</sup> for the sake of consistency of the spectral data between the aromatic and nonaromatic cation based ILs. For this reason, the analytical procedure in this study has been described briefly.

Figure 1a shows the Kerr transient of [Pyr<sub>113</sub>][DCA] from 3.5 fs to 300 ps with the logarithmic scales. Figure 1b illustrates the linear scale in the early time stage, with magnification of the Kerr transient in the time range of  $-0.5$ – $3$  ps. The intensity of the Kerr transient was normalized for the intensity at  $t = 0$ , which is because of the electronic response. The Kerr transient from 3 to 300 ps was analyzed by a triexponential function,  $a_0 + \sum_{i=1}^3 a_i \exp(-t/\tau_i)$ , where  $a_0$  is the offset parameter, and  $a_i$  and  $\tau_i$  are the amplitude and time constant of the  $i$ -th exponential component, respectively. The fit is also given in Figure 1a. The triexponential fit parameters for the present forty nonaromatic cation based ILs are summarized

**Table 1.** Abbreviations and Supplier Sources of ILs Used in This Study.

No.	Abbreviation	Name	Source
1	[N <sub>1113</sub> ][NTf <sub>2</sub> ]	Trimethylpropylammonium bis(trifluoromethylsulfonyl)amide	TCI
2	[N <sub>1224</sub> ][NTf <sub>2</sub> ]	Butyldiethylmethylammonium bis(trifluoromethylsulfonyl)amide	This work
3	[N <sub>1444</sub> ][NTf <sub>2</sub> ]	Tributylmethylammonium bis(trifluoromethylsulfonyl)amide	TCI
4	[N <sub>1444</sub> ][DCA]	Tributylmethylammonium dicyanamide	TCI
5	[N <sub>2228</sub> ][NTf <sub>2</sub> ]	Triethyloctylammonium bis(trifluoromethylsulfonyl)amide	Ref. 61
6	[N <sub>112Bz</sub> ][NTf <sub>2</sub> ]	Benzylethyldimethylammonium bis(trifluoromethylsulfonyl)amide	TCI
7	[N <sub>122(1O2)</sub> ][NTf <sub>2</sub> ]	Diethylmethyl(2-methoxyethyl)ammonium bis(trifluoromethylsulfonyl)amide	Kanto
8	[N <sub>122(1O2)</sub> ][BF <sub>4</sub> ]	Diethylmethyl(2-methoxyethyl)ammonium tetrafluoroborate	Kanto
9	[Pyrr <sub>13</sub> ][NTf <sub>2</sub> ]	1-Methyl-1-propylpyrrolidinium bis(trifluoromethylsulfonyl)amide	This work
10	[Pyrr <sub>13</sub> ][NF <sub>2</sub> ]	1-Methyl-1-propylpyrrolidinium bis(fluorosulfonyl)amide	TCI
11	[Pyrr <sub>13</sub> ][DCA]	1-Methyl-1-propylpyrrolidinium dicyanamide	Iolitec
12	[Pyrr <sub>14</sub> ][NTf <sub>2</sub> ]	1-Butyl-1-methylpyrrolidinium bis(trifluoromethylsulfonyl)amide	Ref. 60
13	[Pyrr <sub>14</sub> ][NF <sub>2</sub> ]	1-Butyl-1-methylpyrrolidinium bis(fluorosulfonyl)amide	Ref. 63
14	[Pyrr <sub>14</sub> ][DCA]	1-Butyl-1-methylpyrrolidinium dicyanamide	TCI
15	[Pyrr <sub>14</sub> ][NPF <sub>2</sub> ]	1-Butyl-1-methylpyrrolidinium bis(pentafluoroethylsulfonyl)amide	Ref. 63
16	[Pyrr <sub>14</sub> ][NCyF]	1-Butyl-1-methylpyrrolidinium cyclohexafluoropropane-1,3-bis(sulfonyl)amide	Ref. 63
17	[Pyrr <sub>14</sub> ][OTf]	1-Butyl-1-methylpyrrolidinium trifluoromethanesulfonate	Ref. 63
18	[Pyrr <sub>14</sub> ][TCM]	1-Butyl-1-methylpyrrolidinium tricyanomethanide	Ref. 63
19	[Pyrr <sub>14</sub> ][FAP]	1-Butyl-1-methylpyrrolidinium tris(perfluoroethyl)trifluorophosphate	Merck
20	[Pyrr <sub>16</sub> ][NTf <sub>2</sub> ]	1-Hexyl-1-methylpyrrolidinium bis(trifluoromethylsulfonyl)amide	This work
21	[Pyrr <sub>18</sub> ][NTf <sub>2</sub> ]	1-Methyl-1-octylpyrrolidinium bis(trifluoromethylsulfonyl)amide	This work
22	[Pyrr <sub>1,10</sub> ][NTf <sub>2</sub> ]	1-Decyl-1-methylpyrrolidinium bis(trifluoromethylsulfonyl)amide	This work
23	[Pyrr <sub>A1</sub> ][NTf <sub>2</sub> ]	1-Allyl-1-methylpyrrolidinium bis(trifluoromethylsulfonyl)amide	TCI
24	[Pyrr <sub>1(1O2)</sub> ][NTf <sub>2</sub> ]	1-(2-Methoxyethyl)-1-methylpyrrolidinium bis(trifluoromethylsulfonyl)amide	Kanto
25	[Pyrr <sub>1(1O2)</sub> ][BF <sub>4</sub> ]	1-(2-Methoxyethyl)-1-methylpyrrolidinium tetrafluoroborate	Kanto
26	[Pyrr <sub>1(1O2)</sub> ][NF <sub>2</sub> ]	1-(2-Methoxyethyl)-1-methylpyrrolidinium bis(fluorosulfonyl)amide	Ref. 63
27	[Pyrr <sub>1(1O2)</sub> ][PF <sub>6</sub> ]	1-(2-Methoxyethyl)-1-methylpyrrolidinium hexafluorophosphate	Ref. 63
28	[Pyrr <sub>1(1O2)</sub> ][NCyF]	1-(2-Methoxyethyl)-1-methylpyrrolidinium cyclohexafluoropropane-1,3-bis(sulfonyl)amide	Wako
29	[Pip <sub>13</sub> ][NTf <sub>2</sub> ]	1-Methyl-1-propylpiperidinium bis(trifluoromethylsulfonyl)amide	Wako
30	[Pip <sub>14</sub> ][NTf <sub>2</sub> ]	1-Butyl-1-methylpiperidinium bis(trifluoromethylsulfonyl)amide	This work
31	[Mor <sub>1(2O2)</sub> ][NTf <sub>2</sub> ]	4-(2-Ethoxyethyl)-4-methylmorpholinium bis(trifluoromethylsulfonyl)amide	Wako
32	[P <sub>1444</sub> ][NTf <sub>2</sub> ]	Tributylmethylphosphonium bis(trifluoromethylsulfonyl)amide	TCI
33	[P <sub>2228</sub> ][NTf <sub>2</sub> ]	Triethyloctylphosphonium bis(trifluoromethylsulfonyl)amide	Ref. 61
34	[P <sub>444,10</sub> ][NTf <sub>2</sub> ]	Tributyldecylphosphonium bis(trifluoromethylsulfonyl)amide	This work
35	[P <sub>444,10</sub> ][NF <sub>2</sub> ]	Tributyldecylphosphonium bis(fluorosulfonyl)amide	This work
36	[P <sub>444,10</sub> ][NPF <sub>2</sub> ]	Tributyldecylphosphonium bis(pentafluoroethylsulfonyl)amide	This work
37	[P <sub>444,10</sub> ][OTf]	Tributyldecylphosphonium trifluoromethanesulfonate	This work
38	[P <sub>222(1S1)</sub> ][NF <sub>2</sub> ]	Triethyl(methylthio)methylphosphonium bis(fluorosulfonyl)amide	Ref. 67
39	[P <sub>444(2S2)</sub> ][BF <sub>4</sub> ]	Tributyl[2-(ethylthio)ethyl]phosphonium tetrafluoroborate	Ref. 67
40	[S <sub>222</sub> ][NTf <sub>2</sub> ]	Triethylsulfonium bis(trifluoromethylsulfonyl)amide	Aldrich

in the Electronic Supporting Information (Table S2-1 of the Electronic Supporting Information). Figure 1c shows the Fourier transform Kerr spectra of [Pyrr<sub>13</sub>][DCA]. The entire spectrum was decomposed into two parts, namely, the overdamped relaxation component (trixponential fit excluded the fast component,  $a_0 + a_2 \exp(-t/\tau_2) + a_3 \exp(-t/\tau_3)$ ) and the spectrum produced by the subtraction of the overdamped relaxation component. Because the relaxation time constants of the first exponential components ( $a_1 \exp(-t/\tau_1)$ ) in the ILs were a few picoseconds, i.e., a similar time scale in the dephasing of typical intramolecular vibrations and the collision- or interaction-induced intermolecular motions, this component was included in the low-frequency spectra in this study (Figure S1 of the Electronic Supporting Information). The broadened band below  $\sim 150 \text{ cm}^{-1}$  in the spectrum without the slow relaxation component was mainly attributed to intermolecular vibrations such as librations (orientational vibrations) and collision- and interaction-induced motions (translational dynamics). It is also noted that the Kerr response was normalized at the intensity at  $t = 0$  in the time domain data, which is the electronic response. Thus the intensities of the spectra are not exactly comparable, but it can be a rough guide



**Figure 1.** (a) Logarithmic plot of the normalized Kerr transient (red line) together with its triexponential fit function (blue line) and (b) short time window transient from  $-0.5$  to  $3.0$  ps for [Pyrr<sub>13</sub>][DCA]. (c) Fourier transform Kerr spectra: entire spectrum (black line), picosecond overdamped relaxation component (blue line), and entire spectrum minus picosecond overdamped relaxation component (red line).

because heavy atoms ( $\geq 4$ th period) are not included in the target ILs in this study.

The line shape of broadened spectral band of each IL, which is mainly due to intermolecular vibrations, was also analyzed. The model function to fit the line shape of the low-frequency spectrum used in this study was a sum of the Ohmic functions ( $I_{O,i}(\omega)$ ),<sup>79</sup>

$$I_{O,i}(\omega) = \sum_{i=1}^n a_{O,i} \omega \exp(-\omega/\omega_{O,i}) \quad (3)$$

where  $a_{O,i}$  and  $\omega_{O,i}$  are the amplitude and characteristic frequency, respectively, of the  $i$ -th Ohmic component, and a sum of anti-symmetrized Gaussian functions ( $I_{G,i}(\omega)$ ),<sup>80</sup>

$$I_{G,i}(\omega) = \sum_{i=1}^n a_{G,i} \left\{ \exp \left[ \frac{-2(\omega - \omega_{G,i})^2}{\Delta\omega_{G,i}^2} \right] - \exp \left[ \frac{-2(\omega + \omega_{G,i})^2}{\Delta\omega_{G,i}^2} \right] \right\} \quad (4)$$

where  $a_{G,i}$ ,  $\omega_{G,i}$ , and  $\Delta\omega_{G,i}$  are the amplitude, characteristic frequency, and width parameter, respectively, of the  $i$ -th

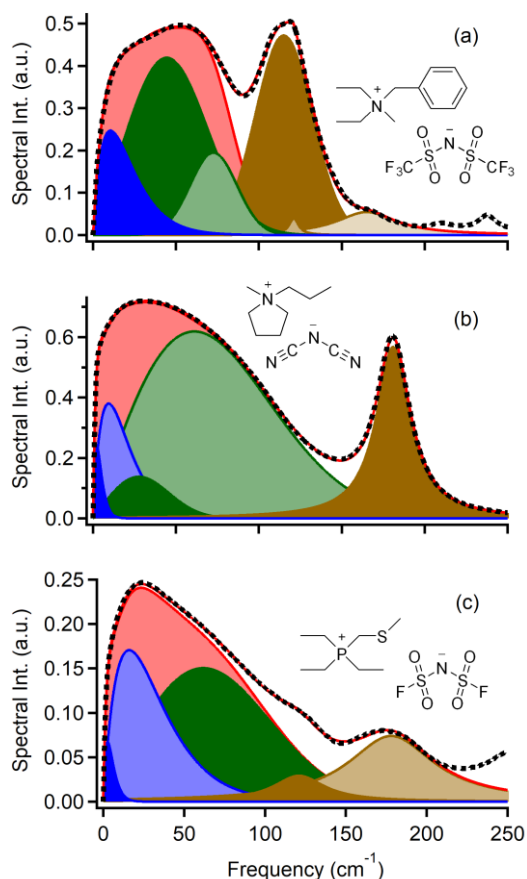


**Figure 2.** Line shape analysis results for the low-frequency Kerr spectra of (a) [N<sub>112B2</sub>][NTf<sub>2</sub>], (b) [Pyrr<sub>13</sub>][DCA], and (c) [P<sub>222(1S1)</sub>][NF<sub>2</sub>]. Black dots denote the experimentally obtained spectra, red lines represent the entire spectral fits, blue areas denote the Ohmic functions, green areas correspond to the anti-symmetrized Gaussian functions (intramolecular vibrational bands), and red areas denote the sums of the Ohmic and anti-symmetrized Gaussian functions.

anti-symmetrized Gaussian function component. When a clear intramolecular vibrational band was observed in the low-frequency spectrum, the band was fitted by a Lorentzian function,

$$I_L(\omega) = \frac{a_L}{(\omega - \omega_L)^2 + \Delta\omega_L^2} \quad (5)$$

where  $a_L$ ,  $\omega_L$ , and  $\Delta\omega_L$  are the amplitude, characteristic frequency, and width parameter, respectively. Figure 2 displays the line shape fits to the low-frequency spectra of [N<sub>112Bz</sub>][NTf<sub>2</sub>], [Pyrr<sub>13</sub>][DCA], and [P<sub>222(1S1)</sub>][NF<sub>2</sub>], as examples. All low-frequency Kerr spectra of the forty nonaromatic cation based ILs were fitted with a similar fit quality. All the low-frequency Kerr spectra of the ILs and the line shape analysis results are summarized in the Electronic Supporting Information (Figure S1). The forty values of the first moment ( $M_1$ ) of each low-frequency spectrum (sum of Ohmic and anti-symmetrized Gaussian components), were defined as,<sup>81</sup>

$$M_1 = \int \omega I(\omega) d\omega / \int I(\omega) d\omega \quad (6)$$

where  $I(\omega)$  is the frequency-dependent intensity of a spectrum that does not include the contributions of the picosecond overdamped relaxations and clear intramolecular vibrational modes. For the present ILs, these intensities were estimated in the frequency region of 0–1000 cm<sup>-1</sup> and are listed in Table 2.

In the line shape analysis (Figure 2), each function is not infallible to assign a band to its origin vibrational mode, unlike common intramolecular vibrational modes. This is because the intermolecular vibrations overlap in the frequency region (as well as the time region), and the vibrational bands in the liquid phase are broad in comparison with the intermolecular vibrational band in the gas phase. In addition, the intermolecular vibrational modes in liquids and solutions are often coupled with each other. Molecular dynamics (MD) simulations indicate that the cross-term (or coupling term) of different kinds of intermolecular vibrations in both molecular liquids<sup>82,83</sup> and ILs provides either a positive or negative intensity depending on the target system.<sup>84–86</sup> Although there have been attempts to obtain a more realistic feature from the line shape analysis of the low-frequency spectrum in molecular liquids,<sup>13,87,88</sup> the purposes of the line shape analysis in this study are removing the contributions of clear intramolecular vibrational modes from a broad spectrum, estimating  $M_1$  of the spectrum, and representing the low-frequency spectrum quantitatively for overview of the intermolecular vibrational bands of the forty nonaromatic cation based ILs.

## 4. Results and Discussion

### 4.1 Bulk Liquid Properties

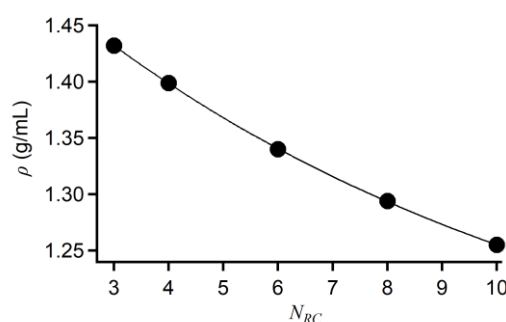
**4.1.1 Density  $\rho$ :** The  $\rho$  values for the forty nonaromatic cation based ILs at 293 K estimated in this study are summarized in Table 2. The  $\rho$  values of the ILs at 293 K and/or near temperatures from previous reports<sup>41,61,67,89–115</sup> are also given in Table 2. The  $\rho$  values measured in this study were quite similar to the reported values, i.e., within experimental errors if we consider the effect of temperature on the liquid density. The  $\rho$  data of some ILs (e.g., [Pyrr<sub>1(102)</sub>][NCyF], [P<sub>444,10</sub>][NF<sub>2</sub>], and so on) have not been reported to date, to the best of our knowledge.

Figure 3 shows the plot of  $\rho$  versus the number of carbons of the alkyl group,  $N_{RC}$ , of 1-alkyl-1-methylpyrrolidinium cations ([Pyrr<sub>1n</sub>]<sup>+</sup>,  $n = N_{RC}$ ) for the bis(trifluoromethylsulfonyl)amide ([NTf<sub>2</sub>]<sup>-</sup>) salts ([Pyrr<sub>13</sub>][NTf<sub>2</sub>], [Pyrr<sub>14</sub>][NTf<sub>2</sub>], [Pyrr<sub>16</sub>][NTf<sub>2</sub>], [Pyrr<sub>18</sub>][NTf<sub>2</sub>],

and [Pyrr<sub>1,10</sub>][NTf<sub>2</sub>]). It is evident from the figure that the  $\rho$  value of [Pyrr<sub>1n</sub>][NTf<sub>2</sub>] series decreased with the increasing length of the alkyl group. This is a rather general feature of liquid density in not only pyrrolidinium-based ILs, but also other ILs such as imidazolium-based and pyridinium-based ILs.<sup>19,59,116</sup> Previously, we showed the linear relations between  $\rho$  and  $N_{RC}$  for 1-alkyl-3-methylimidazolium bis(trifluoromethylsulfonyl)amides, [C<sub>n</sub>MIm][NTf<sub>2</sub>] ( $n = 2–10$ ), *N*-alkylpyridinium bis(trifluoromethylsulfonyl)amides, [C<sub>n</sub>Py][NTf<sub>2</sub>] ( $n = 4–12$ ), and 1-alkyl-3-methylimidazolium tetrafluoroborates, [C<sub>n</sub>MIm][BF<sub>4</sub>] ( $n = 2–10$ ).<sup>59</sup> The alkyl group dependence of  $\rho$  in [Pyrr<sub>1n</sub>][NTf<sub>2</sub>] is, however, represented by an exponential function, as shown in Figure 3:

$$\rho \text{ (g mL}^{-1}\text{)} = 1.086 + 0.4700 \exp(-0.1027N_{RC}) \quad (7)$$

where  $N_{RC}$  is the number of carbons of the alkyl group in the cation. As the nonlinearity of  $\rho$  in relation to  $N_{RC}$  for [Pyrr<sub>1n</sub>][NTf<sub>2</sub>] was not significant, it is possible that we missed the nonlinear behavior of  $\rho$  with respect to  $N_{RC}$  for the aromatic cation based ILs in that study.<sup>59</sup>



**Figure 3.** Plots of liquid density,  $\rho$ , vs. number of carbons of the alkyl group in [Pyrr<sub>1n</sub>]<sup>+</sup>,  $N_{RC}$ , for [Pyrr<sub>13</sub>][NTf<sub>2</sub>], [Pyrr<sub>14</sub>][NTf<sub>2</sub>], [Pyrr<sub>16</sub>][NTf<sub>2</sub>], [Pyrr<sub>18</sub>][NTf<sub>2</sub>], and [Pyrr<sub>1,10</sub>][NTf<sub>2</sub>]. Fit curve by an exponential function is also indicated by a solid curve.

Figure 4 shows the plot of  $\rho$  vs. the total number of carbons of the alkyl and aromatic groups of [N<sub>1113</sub>][NTf<sub>2</sub>], [N<sub>1224</sub>][NTf<sub>2</sub>], [N<sub>1444</sub>][NTf<sub>2</sub>], [N<sub>2228</sub>][NTf<sub>2</sub>], and [N<sub>112Bz</sub>][NTf<sub>2</sub>]. Note that Figure 4 shows the plot for the total number of carbons of cations, but Figure 3 is for the number of carbons of only the alkyl groups in the cations. It is clear from Figure 4 that the  $\rho$  values of the ammonium-based ILs depended on the total number of carbons of the cation, except for [N<sub>112Bz</sub>][NTf<sub>2</sub>]. This was attributed to the nature of the compact (or dense) structure of the phenyl ring. The dependence of  $\rho$  on the total number of carbons of the cations in the ammonium-based ILs with [NTf<sub>2</sub>]<sup>-</sup>, except for [N<sub>112Bz</sub>][NTf<sub>2</sub>], is given as follows:

$$\rho \text{ (g mL}^{-1}\text{)} = 0.8794 + 0.7568 \exp(-0.05176N_C) \quad (8)$$

Comparing the  $\rho$  values of [N<sub>1224</sub>][NTf<sub>2</sub>], [Pyrr<sub>14</sub>][NTf<sub>2</sub>], and [Pip<sub>13</sub>][NTf<sub>2</sub>] provides an insight into the effect of the structures of cation skeletons on the density, because the number of carbons of the cations is the same. The trend of decreasing influence on density is as follows: [Pip<sub>13</sub>]<sup>+</sup> > [Pyrr<sub>14</sub>]<sup>+</sup> > [N<sub>1224</sub>]<sup>+</sup>. A comparison of the  $\rho$  values of the ammonium-based ILs, [N<sub>1444</sub>][NTf<sub>2</sub>] and [N<sub>2228</sub>][NTf<sub>2</sub>], and their respective phosphonium-based ILs, [P<sub>1444</sub>][NTf<sub>2</sub>] and [P<sub>2228</sub>][NTf<sub>2</sub>], revealed that the densities of the ammonium-based ILs, [N<sub>1444</sub>][NTf<sub>2</sub>] and [N<sub>2228</sub>][NTf<sub>2</sub>], and their respective phosphonium-based ILs, [P<sub>1444</sub>][NTf<sub>2</sub>] and

**Table 2.** Physical Properties of Nonaromatic ILs at 293 K.

No.	Ionic Liquid	FW (g/mol)	$\rho$ (g/mL)	$V_m$ (mL/mol)	$\eta$ (cP)	$\sigma$ (mS/cm)	$A$ (Scm <sup>2</sup> /mol)	$\gamma$ (mN/m)	$M_1$ (cm <sup>-1</sup> )	H <sub>2</sub> O Cont. (ppm)
1	[N <sub>1113</sub> ][NTf <sub>2</sub> ]	382.34	1.433 (1.430 <sup>e89</sup> , 1.43 <sup>d90</sup> )	267	95.3 (78.1 <sup>e89</sup> , 95 <sup>a117</sup> )	1.89 (3.03 <sup>e89</sup> , 3.24 <sup>d90</sup> )	0.504	34.4 (35.1 <sup>i118</sup> )	44.0	42
2	[N <sub>1224</sub> ][NTf <sub>2</sub> ]	424.42	1.358 (1.34 <sup>a91</sup> , 1.38 <sup>d92</sup> )	313	157 (161 <sup>a91</sup> , 120 <sup>d92</sup> )	1.22 (1.0 <sup>a91</sup> , 1.6 <sup>d92</sup> )	0.381	33.6	49.7	50
3	[N <sub>1444</sub> ][NTf <sub>2</sub> ]	480.53	1.265 (1.270 <sup>a93</sup> , 1.267 <sup>94</sup> )	380	784 (819.2 <sup>94</sup> )	0.464 (2.10 <sup>i119</sup> )	0.176	30.8 (30.6 <sup>i93</sup> )	52.9	91
4	[N <sub>1444</sub> ][DCA]	266.43	0.948 (0.98 <sup>d95</sup> )	281	407 (410 <sup>d95</sup> )	0.783 (0.57 <sup>d95</sup> )	0.220	44.1	65.4	35
5	[N <sub>2228</sub> ][NTf <sub>2</sub> ]	494.55	1.253 (1.249 <sup>b61</sup> , 1.251 <sup>c96</sup> )	395	211 (227.0 <sup>b61</sup> , 221.4 <sup>c96</sup> )	0.595 (0.33 <sup>d120</sup> )	0.235	32.0 (32.8 <sup>b61</sup> , 33.1 <sup>c96</sup> )	49.4	41
6	[N <sub>112Bz</sub> ][NTf <sub>2</sub> ]	444.41	1.429	311	650	0.441	0.137	37.7	47.2	56
7	[N <sub>122(102)</sub> ][NTf <sub>2</sub> ]	426.39	1.413 (1.42 <sup>d92</sup> , 1.407 <sup>d97</sup> )	302	88.8 (69 <sup>d92</sup> , 70.96 <sup>d97</sup> )	2.06 (2.6 <sup>d92</sup> )	0.622	35.0 (33.6 <sup>d97</sup> )	49.6	82
8	[N <sub>122(102)</sub> ][BF <sub>4</sub> ]	233.06	1.182 (1.20 <sup>d92</sup> )	197	544 (426 <sup>d92</sup> )	1.26 (1.3 <sup>d92</sup> )	0.248	50.6	72.0	61
9	[Pyrr <sub>13</sub> ][NTf <sub>2</sub> ]	408.37	1.432 (1.434 <sup>c98</sup> , 1.432 <sup>a99</sup> )	285	69.5 (63 <sup>c121</sup> , 72 <sup>a99</sup> )	2.86 (3.6 <sup>c121</sup> , 2.20 <sup>a99</sup> )	0.816	35.3 (34.4 <sup>d108</sup> )	45.2	63
10	[Pyrr <sub>13</sub> ][NF <sub>2</sub> ]	308.36	1.343 (1.339 <sup>c98</sup> )	230	47.1 (40 <sup>c122</sup> , 39 <sup>a123</sup> )	4.91 (6.4 <sup>c122</sup> , 9.14 <sup>a123</sup> )	1.13	47.9	44.7	22
11	[Pyrr <sub>13</sub> ][DCA]	194.28	1.029 (1.038 <sup>a100</sup> )	189	28.7 (33.2 <sup>a100</sup> , 27.1 <sup>a124</sup> )	8.18 (15.7 <sup>a124</sup> )	1.55	57.3	63.9	78
12	[Pyrr <sub>14</sub> ][NTf <sub>2</sub> ]	422.40	1.399 (1.396 <sup>c89</sup> , 1.399 <sup>a99</sup> )	302	96.4 (97.1 <sup>63</sup> , 95 <sup>a99</sup> )	1.96 (2.84 <sup>f125</sup> , 1.77 <sup>a99</sup> )	0.592	33.6 (33.0 <sup>d108</sup> )	46.8	29
13	[Pyrr <sub>14</sub> ][NF <sub>2</sub> ]	322.39	1.311 (1.311 <sup>a101</sup> , 1.306 <sup>d102</sup> )	246	62.1 (61.4 <sup>63</sup> , 64.13 <sup>a101</sup> )	5.72 (5.25 <sup>a101</sup> )	1.41	44.6 (35.04 <sup>d102</sup> )	47.0	47
14	[Pyrr <sub>14</sub> ][DCA]	208.31	1.015 (1.013 <sup>d103</sup> )	205	36.8 (36.5 <sup>d103</sup> , 38.8 <sup>63</sup> )	6.63 (10.1 <sup>a124</sup> )	1.36	53.0 (56.2 <sup>k126</sup> )	64.0	68
15	[Pyrr <sub>14</sub> ][NPF <sub>2</sub> ]	522.42	1.480 (1.481 <sup>a99</sup> )	353	324 (341.0 <sup>63</sup> , 350 <sup>a99</sup> )	0.671 (0.774 <sup>f125</sup> , 0.42 <sup>a99</sup> )	0.237	30.1	44.9	41
16	[Pyrr <sub>14</sub> ][NCyF]	434.41	1.449	300	459 (486 <sup>63</sup> )	0.716 (0.35 <sup>a127</sup> )	0.225	34.1	49.0	20
17	[Pyrr <sub>14</sub> ][OTf]	291.33	1.256 (1.256 <sup>a104</sup> , 1.256 <sup>a105</sup> )	232	222 (227 <sup>63</sup> , 221.7 <sup>a39</sup> )	1.67 (1.3 <sup>a105</sup> )	0.387	36.4	65.9	47
18	[Pyrr <sub>14</sub> ][TCM]	232.32	1.008 (1.001 <sup>i106</sup> , 1.01 <sup>d107</sup> )	230	30.4 (33.0 <sup>63</sup> , 29.0 <sup>d42</sup> )	5.55 (8.7 <sup>d107</sup> )	1.28	51.1 (48.04 <sup>i106</sup> )	54.9	68
19	[Pyrr <sub>14</sub> ][FAP]	587.28	1.588 (1.580 <sup>d103</sup> , 1.589 <sup>a43</sup> )	370	260 (221.0 <sup>d103</sup> , 288 <sup>63</sup> )	1.10 (1.053 <sup>d128</sup> )	0.407	33.7 (35.0 <sup>a129</sup> )	41.3	44
20	[Pyrr <sub>16</sub> ][NTf <sub>2</sub> ]	450.46	1.340 (1.32 <sup>d108</sup> )	336	137 (133.2 <sup>a130</sup> )	1.13 (1.0 <sup>a131</sup> , 1.2 <sup>a130</sup> )	0.380	32.0 (31.7 <sup>d108</sup> )	47.2	69

21	[Pyrr <sub>18</sub> ][NTf <sub>2</sub> ]	478.51	1.294 (1.289 <sup>d109</sup> )	370	178 (138.17 <sup>d109</sup> )	0.787 (0.54 <sup>a131</sup> )	0.291	31.6	46.9	76
22	[Pyrr <sub>1,10</sub> ][NTf <sub>2</sub> ]	506.56	1.255 (1.25 <sup>d108</sup> )	404	239 (150 <sup>d108</sup> )	0.585 (0.37 <sup>a131</sup> )	0.236	31.8 (31.4 <sup>d108</sup> )	49.2	37
23	[Pyrr <sub>A1</sub> ][NTf <sub>2</sub> ]	406.36	1.454 (1.447 <sup>m110</sup> )	279	70.9 (52 <sup>c121</sup> , 39.5 <sup>m110</sup> )	2.49 (3.7 <sup>c121</sup> , 4.2 <sup>m110</sup> )	0.696	36.1	42.4	35
24	[Pyrr <sub>1(102)</sub> ][NTf <sub>2</sub> ]	424.37	1.458 (1.46 <sup>g41</sup> , 1.459 <sup>a99</sup> )	291	64.4 (64.0 <sup>g3</sup> , 62 <sup>a99</sup> )	3.26 (3.88 <sup>d132</sup> , 3.45 <sup>d27</sup> )	0.949	35.9 (35.26 <sup>d132</sup> )	49.2	70
25	[Pyrr <sub>1(102)</sub> ][BF <sub>4</sub> ]	231.04	1.234 (1.235 <sup>d111</sup> )	187	217 (232 <sup>g3</sup> , 213 <sup>d111</sup> )	2.59 (2.9 <sup>d111</sup> )	0.485	52.6	68.9	74
26	[Pyrr <sub>1(102)</sub> ][NF <sub>2</sub> ]	324.36	1.379	235	47.0 (47.9 <sup>g3</sup> , 43.6 <sup>n133</sup> )	4.65 (7.66 <sup>n133</sup> )	1.09	47.9	51.1	71
27	[Pyrr <sub>1(102)</sub> ][PF <sub>6</sub> ]	289.20	1.397	207	768 (753 <sup>g3</sup> )	0.587	0.122	50.7	70.2	36
28	[Pyrr <sub>1(102)</sub> ][NCyF]	436.38	1.510	289	289 (308 <sup>g3</sup> )	0.688	0.199	35.4	56.5	42
29	[Pip <sub>13</sub> ][NTf <sub>2</sub> ]	422.40	1.414 (1.414 <sup>e89</sup> , 1.416 <sup>a94</sup> )	299	184 (145.8 <sup>e89</sup> , 198.1 <sup>a94</sup> )	1.21 (1.58 <sup>e89</sup> )	0.361	35.8 (34.4 <sup>i118</sup> , 35.6 <sup>o94</sup> )	46.3	36
30	[Pip <sub>14</sub> ][NTf <sub>2</sub> ]	436.43	1.384 (1.38 <sup>d93</sup> , 1.38 <sup>d112</sup> )	315	253 (183 <sup>d112</sup> , 247.7 <sup>a94</sup> )	1.03 (1.11 <sup>d90</sup> , 1.2 <sup>d112</sup> )	0.325	34.2 (34.5 <sup>p94</sup> )	46.9	44
31	[Mor <sub>1(202)</sub> ][NTf <sub>2</sub> ]	454.40	1.464 (1.46 <sup>d112</sup> )	310	341 (298 <sup>d112</sup> )	0.643 (1.1 <sup>d112</sup> )	0.200	35.1	47.2	34
32	[P <sub>1444</sub> ][NTf <sub>2</sub> ]	497.49	1.259 (1.28 <sup>d113</sup> )	395	352 (207 <sup>d113</sup> )	0.576 (0.42 <sup>d113</sup> )	0.228	30.7	52.7	33
33	[P <sub>2228</sub> ][NTf <sub>2</sub> ]	511.52	1.249 (1.244 <sup>b61</sup> , 1.244 <sup>d114</sup> )	410	151 (123.3 <sup>b61</sup> , 119.42 <sup>d114</sup> )	0.797 (0.891 <sup>d114</sup> )	0.326	31.6 (32.7 <sup>b61</sup> )	53.5	76
34	[P <sub>444,10</sub> ][NTf <sub>2</sub> ]	623.74	1.146 (1.142 <sup>d114</sup> )	544	324 (301.06 <sup>d114</sup> )	0.415 (0.226 <sup>d114</sup> )	0.226	30.2	54.0	90
35	[P <sub>444,10</sub> ][NF <sub>2</sub> ]	523.72	1.077	486	438	0.408	0.198	34.4	52.7	77
36	[P <sub>444,10</sub> ][NPF <sub>2</sub> ]	723.75	1.211	598	647	0.347	0.207	28.0	53.5	56
37	[P <sub>444,10</sub> ][OTf]	492.66	1.041	473	900	0.327	0.155	30.5	62.8	50
38	[P <sub>222(1S1)</sub> ][NF <sub>2</sub> ]	359.40	1.344 (1.344 <sup>g7</sup> )	267	58.4 (58.2 <sup>g7</sup> )	2.61 (2.925 <sup>g7</sup> )	0.698	47.8 (47.2 <sup>g7</sup> )	56.1	72
39	[P <sub>444(2S2)</sub> ][BF <sub>4</sub> ]	378.30	1.075 (1.076 <sup>g7</sup> )	352	1825 (1847 <sup>g7</sup> )	0.337 (0.332 <sup>g7</sup> )	0.119	35.4 (36.6 <sup>g7</sup> )	60.6	89
40	[S <sub>222</sub> ][NTf <sub>2</sub> ]	399.38	1.465 (1.46 <sup>a115</sup> , 1.467 <sup>94</sup> )	273	37.9 (41.1 <sup>a94</sup> , 30 <sup>d134</sup> )	4.88 (7.1 <sup>d134</sup> )	1.33	35.4 (35.5 <sup>p94</sup> )	56.0	46

<sup>a</sup> Data at 293.15 K. <sup>b</sup> Data at 297 K. <sup>c</sup> Data at 298 K. <sup>d</sup> Data at 298.15 K. <sup>e</sup> Data at 298.2 K. <sup>f</sup> Data at 305 K. <sup>g</sup> Data at 295K. <sup>h</sup> Data at 296K. <sup>i</sup> Data at 294.399 K.

<sup>j</sup> Data at 303 K. <sup>k</sup> Data at 293.05 K. <sup>l</sup> Data at 308.15 K. <sup>m</sup> Data at 303.15 K. <sup>n</sup> Data at 296.15 K. <sup>o</sup> Data at 293.4 K. <sup>p</sup> Data at 293 K.

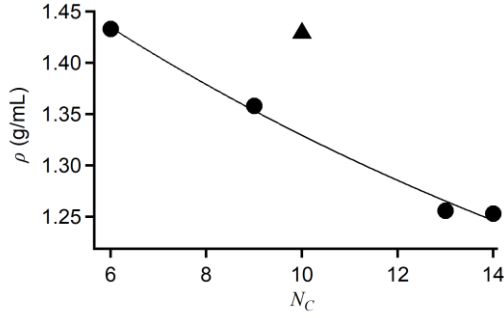


**Figure 4.** Plot of liquid density  $\rho$  vs. total number of carbons of the cations  $N_c$  for  $[\text{N}_{1113}][\text{NTf}_2]$ ,  $[\text{N}_{1224}][\text{NTf}_2]$ ,  $[\text{N}_{1444}][\text{NTf}_2]$ ,  $[\text{N}_{2228}][\text{NTf}_2]$  (circles), and  $[\text{N}_{112\text{Bz}}][\text{NTf}_2]$  (triangle). Fit curve by an exponential function for  $[\text{N}_{1113}][\text{NTf}_2]$ ,  $[\text{N}_{1224}][\text{NTf}_2]$ ,  $[\text{N}_{1444}][\text{NTf}_2]$ , and  $[\text{N}_{2228}][\text{NTf}_2]$  is also given.

$[\text{P}_{2228}][\text{NTf}_2]$ , revealed that the densities of the phosphonium-based ILs were slightly higher than those of the respective ammonium-based ILs. Tsunashima and Sugiya,<sup>135</sup> as well as our group,<sup>61</sup> have previously reported similar density behavior of phosphonium-based ILs as compared to ammonium-based ILs. It is also noteworthy that the substitution of an alkyl group in the cations with its respective ether group (e.g.,  $[\text{Pyrr}_{1(102)}]^+$  vs.  $[\text{Pyrr}_{14}]^+$ ) gives a higher density in ILs. This is a rather general feature of the ether group substitution effect of cations on the density of ILs, as well as (neutral) molecular liquids.<sup>19,136</sup>

Regarding anion species, we compared the  $\rho$  values of the 1-butyl-1-methylpyrrolidinium ( $[\text{Pyrr}_{14}]^+$ )-based ILs with eight anions in this study, as shown in Table 2. The decreasing trend of densities of the anion species was:  $[\text{FAP}]^- > [\text{NPF}_2]^- > [\text{NCyF}]^- > [\text{NTf}_2]^- > [\text{NF}_2]^- > [\text{OTf}]^- > [\text{DCA}]^- \sim [\text{TCM}]^-$ . In addition, it was evident from the  $\rho$  data of the 1-methoxyethyl-1-methylpyrrolidinium-based ILs that  $[\text{PF}_6]^-$  was likely in between  $[\text{NTf}_2]^-$  and  $[\text{NF}_2]^-$ , and  $[\text{BF}_4]^-$  was in between  $[\text{OTf}]^-$  and  $[\text{DCA}]^-$  or  $[\text{TCM}]^-$ .

**4.1.2 Viscosity  $\eta$ :** The viscosity data at 293 K for the present ILs are given in Table 2. The  $\eta$  values of the ILs reported in preceding works are also listed in Table 2.<sup>61,63,67,89,91,92,94-97,99-101,103,108-114,117,121-124,130,133,134</sup> The reported  $\eta$  values of the ILs were in a good agreement with those estimated in this study (within the range of experimental error), taking the effect of temperature into consideration overall.

It is known that the viscosity in ILs depends strongly on the length of the alkyl group of cations.<sup>19</sup> The pyrrolidinium-based ILs with  $[\text{NTf}_2]^-$  studied here also showed this viscosity behavior. Figure 5 shows the semi-logarithmic plots of  $\eta$  vs.  $N_{RC}$  for  $[\text{Pyrr}_{1n}][\text{NTf}_2]$ . The relation between  $\eta$  and  $N_{RC}$  is:

$$\log(\eta \text{ (cP)}) = 1.664 + 0.07323N_{RC} \quad (9)$$

The slope for  $[\text{Pyrr}_{1n}][\text{NTf}_2]$  was found to be close to that for  $[\text{C}_n\text{MIm}][\text{NTf}_2]$  ( $\log(\eta \text{ (cP)}) = 1.457 + 0.07404N_{RC}$ ), but the viscosity at the intercept for  $[\text{Pyrr}_{1n}][\text{NTf}_2]$  was similar to that of  $[\text{C}_n\text{Py}][\text{NTf}_2]$  ( $\log(\eta \text{ (cP)}) = 1.628 + 0.06392N_{RC}$ ).

In terms of the effect of the total number of carbons of the ammonium cations, except for  $[\text{N}_{112\text{Bz}}]^+$ , on the viscosity, there was no simple  $N_c$  dependence of  $\eta$  evident for  $[\text{N}_{1113}][\text{NTf}_2]$ ,  $[\text{N}_{1224}][\text{NTf}_2]$ ,  $[\text{N}_{1444}][\text{NTf}_2]$ , and  $[\text{N}_{2228}][\text{NTf}_2]$  in Table 2. It seems that the van der Waals interactions originating from the bulky cation strongly affected the viscosity in  $[\text{N}_{1444}][\text{NTf}_2]$ .

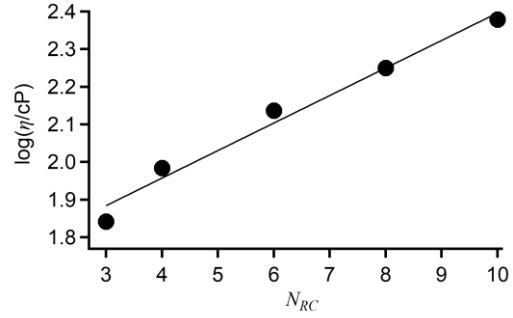


**Figure 5.** Semi-logarithmic plots of viscosity,  $\eta$ , vs. number of carbons of alkyl group in  $[\text{Pyrr}_{1n}]^+$ ,  $N_{RC}$ , for  $[\text{Pyrr}_{13}][\text{NTf}_2]$ ,  $[\text{Pyrr}_{14}][\text{NTf}_2]$ ,  $[\text{Pyrr}_{16}][\text{NTf}_2]$ ,  $[\text{Pyrr}_{18}][\text{NTf}_2]$ , and  $[\text{Pyrr}_{1,10}][\text{NTf}_2]$ . The fit curve is indicated by a black line.

Substitution of an alkyl group of the cation with the respective alkoxyalkyl group reduced the IL viscosity, as shown in Table 2. Comparison of the IL viscosities of the ammonium and phosphonium cations ( $[\text{N}_{1444}]^+$  vs.  $[\text{P}_{1444}]^+$  and  $[\text{N}_{2228}]^+$  vs.  $[\text{P}_{2228}]^+$ ) revealed a substantial reduction in the viscosity for the phosphonium-based ILs. Further, it was evident from the data in Table 2 that the pyrrolidinium-based ILs had a lower viscosity than their corresponding piperidinium-based ILs (e.g.,  $[\text{Pyrr}_{14}][\text{NTf}_2]$  vs.  $[\text{Pip}_{13}][\text{NTf}_2]$  or  $[\text{Pip}_{14}][\text{NTf}_2]$ ).

It is also known that the viscosity of an IL depends strongly on the anion species. The trend of decreasing  $\eta$  in the  $[\text{Pyrr}_{14}]^+$ -based ILs with eight different anions in this study was:  $[\text{NCyF}]^- > [\text{NPF}_2]^- > [\text{FAP}]^- > [\text{OTf}]^- > [\text{NTf}_2]^- > [\text{NF}_2]^- > [\text{DCA}]^- > [\text{TCM}]^-$ .

**4.1.3 Electrical Conductivity  $\sigma$ :** The  $\sigma$  data of the forty nonaromatic cation based ILs are summarized in Table 2. The  $\sigma$  values of the ILs reported previously are also given in Table 2 as references.<sup>67,89-92,95,99,101,105,107,110-114,119-125,127,128,130-134,137</sup> The molar electrical conductivities  $\Lambda$ , defined as  $\sigma V_m$ , are also given in Table 2. Figure 6 shows (a) plots of  $\sigma$  vs.  $\eta^{-1}$  and (b) logarithmic plots of  $\Lambda$  vs.  $\eta^{-1}$  for the forty nonaromatic cation based ILs in this study. In addition, the data for the forty aromatic cation-ILs in our previous work<sup>13</sup> are also plotted in Figure 6. It is clear from Figure 6a that the plots for the ILs show almost linear relationships between  $\sigma$  and  $\eta^{-1}$ . The relations between the electrical conductivity  $\sigma$  and  $\eta^{-1}$  for different types of ILs are:

$$\sigma \text{ (mS/cm)} = 205\eta^{-1} \text{ (cP}^{-1}\text{)} + 0.118 \quad \text{(nonaromatic cation based ILs)} \quad (10)$$

$$\sigma \text{ (mS/cm)} = 292\eta^{-1} \text{ (cP}^{-1}\text{)} - 0.068 \quad \text{(aromatic cation based ILs)} \quad (11)$$

For both types ILs,

$$\sigma \text{ (mS/cm)} = 256\eta^{-1} \text{ (cP}^{-1}\text{)} + 0.001 \quad \text{(both ILs)} \quad (12)$$

The relations between the molar electrical conductivity  $\Lambda$  and  $\eta^{-1}$  are analyzed by the fractional Walden rule:<sup>138</sup>

$$\Lambda \text{ (Scm}^2\text{/mol)} = 19.5[\eta^{-1} \text{ (cP}^{-1}\text{)}]^{0.753} \quad \text{(nonaromatic cation based ILs)} \quad (13)$$

$$\Lambda \text{ (Scm}^2\text{/mol)} = 46.6[\eta^{-1} \text{ (cP}^{-1}\text{)}]^{0.911} \quad \text{(aromatic cation based ILs)} \quad (14)$$

$$\Lambda \text{ (Scm}^2\text{/mol)} = 36.2[\eta^{-1} \text{ (cP}^{-1})]^{0.872} \quad (15)$$

(both ILs)

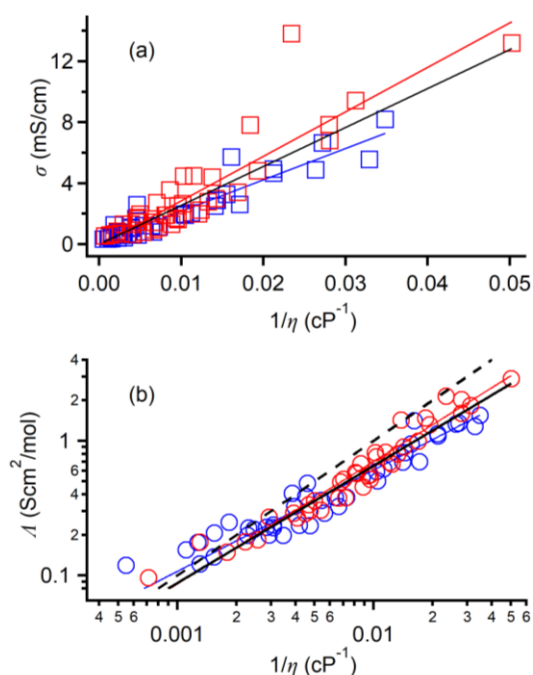


**Figure 6.** (a) Plots of  $\sigma$  vs.  $\eta^{-1}$  and (b) logarithmic plots of  $\Lambda$  vs.  $\eta^{-1}$  for forty nonaromatic cation based ILs studied here (blue symbols). Data for forty aromatic cation based ILs reported in Ref. 59 are also given (red symbols). Fit curves for nonaromatic and aromatic cation based ILs are shown by red and blue lines, respectively. Fits for all data of nonaromatic and aromatic cation based ILs are given by black lines. Black dashed line denotes the ideal Walden line with the unity slope.

It is evident from Figure 6 that the slopes in the plots for the aromatic cation based ILs are slightly steeper than those for the nonaromatic cation based ILs, i.e., the electrical conductivity was more sensitive to the viscosity of the aromatic cation based ILs than that of the nonaromatic cation based ILs. This implied that the nonaromatic cation based ILs required lower viscosity to achieve the same molar electrical conductivity as the aromatic cation based ILs. Watanabe and coworkers have reported a larger value of the ratio of the molar conductivities estimated by electrical conductivity and NMR measurements for nonaromatic cation based ILs (butyltrimethylammonium bis(trifluoromethylsulfonyl)amide and [Pyrr<sub>14</sub>][NTf<sub>2</sub>]) than that for aromatic cation based ILs (1-butyl-3-methylimidazolium bis(trifluoromethylsulfonyl)amide and *N*-butylpyridinium bis(trifluoromethylsulfonyl)amide).<sup>139</sup> Because the value of the ratio of the molar conductivities estimated by electrical conductivity and NMR measurements is essentially related to the percentage of ions (charged species) contributing to the ionic conduction in the diffusing species, nonaromatic cation based ILs are more ionic in nature than aromatic cation based ILs. Therefore, the results in Figure 6 indicate that a higher ionicity increases the viscosity of ILs. It looks that this tendency is clearer in the higher viscosity region, as shown in Figure 6b. The analysis results based on the fractional Walden rule<sup>138</sup> also show that the exponent value is farer from unity for nonaromatic cation based ILs than aromatic cation based ILs. This implies that nonaroma cation based ILs tend to be more decoupled between the electrical conductivity and viscosity

than aromatic cation based ILs.

In addition to the overall picture of the electrical conductivities of nonaromatic cation based ILs, the  $N_{RC}$  dependence of  $\sigma$  for the 1-alkyl-1-methylpyrrolidinium bis(trifluoromethylsulfonyl)amide, [Pyrr<sub>1*n*][NTf<sub>2</sub>], series is shown in Figure 7. Note that Figure 7 shows semi-logarithmic plots. It is clear from the figure that  $\sigma$  decreases with the increasing length of the alkyl group for the [Pyrr<sub>1*n*][NTf<sub>2</sub>] series. As seen in Figure 7, the  $\sigma$  and  $\Lambda$  values do not simply express an exponential feature. Previously, a variant of the Vogel-Tammann-Fulcher (VTF) equation<sup>140-143</sup> was used to express the  $N_{RC}$  dependence of  $\sigma$  and  $\Lambda$  for 1-alkyl-1-methylimidazolium-based ILs with bis(trifluoromethylsulfonyl)amide and tetrafluoroborate anions and [C<sub>*n*</sub>Py][NTf<sub>2</sub>].<sup>59</sup> The results for [Pyrr<sub>1*n*][NTf<sub>2</sub>] also showed the VTF-type behavior in electrical conductivity and molar electrical conductivity:</sub></sub></sub>

$$\sigma = \sigma_0 \exp[B/(N_{RC} - N_{RC,0})] \quad (16)$$

$$\Lambda = \Lambda_0 \exp[B'/(N_{RC} - N'_{RC,0})] \quad (17)$$

where  $\sigma_0$  is the limiting electrical conductivity,  $B$  is a constant that is related to a parameter of the carbon number sensitivity to  $\sigma$ , and  $N_{RC,0}$  is a constant that could be the critical carbon number of the alkyl group where the electrical conductivity diverges,  $\Lambda_0$  is the limiting molar electrical conductivity,  $B'$  is a constant related to a parameter of the carbon number sensitivity to  $\Lambda$  and  $N'_{RC,0}$  is a constant that could be the critical carbon number of the alkyl group where the molar electrical conductivity diverges. The fit parameters obtained for [Pyrr<sub>1*n*][NTf<sub>2</sub>] were:  $\sigma_0 = 0.0949$  (mS/cm),  $B = 12.0$ , and  $N_{RC,0} = -5.09$ ,  $\Lambda_0 = 0.0781$  (Scm<sup>2</sup>/mol),  $B' = 6.40$ , and  $N'_{RC,0} = -3.28$ . From the comparison with the parameters of [C<sub>*n*</sub>MIm][NTf<sub>2</sub>]s and [C<sub>*n*</sub>Py][NTf<sub>2</sub>],  $B$  and  $B'$  for [Pyrr<sub>1*n*][NTf<sub>2</sub>] are slightly low, as well as  $N_{RC,0}$  and  $N'_{RC,0}$ . This indicates that the (molar) electrical conductivity for the [Pyrr<sub>1*n*][NTf<sub>2</sub>] series was less sensitive to the alkyl group and possess the larger critical carbon number of the alkyl group.</sub></sub></sub>

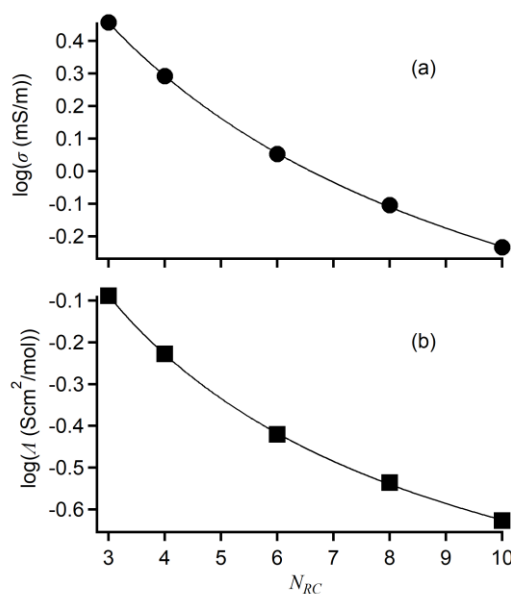


**Figure 7.** Plots of (a)  $\log(\sigma)$  vs.  $N_{RC}$  and (b)  $\log(\Lambda)$  vs.  $N_{RC}$  for [Pyrr<sub>1*n*][NTf<sub>2</sub>]. The VTF fit curves are also shown by solid lines.</sub>

The decreasing trend of  $\sigma$  with respect to the eight anions in the [Pyrr<sub>14</sub>]<sup>+</sup>-based ILs in this study was found to be: [DCA]<sup>-</sup> > [NF<sub>2</sub>]<sup>-</sup> > [TCM]<sup>-</sup> > [NTf<sub>2</sub>]<sup>-</sup> > [OTf]<sup>-</sup> > [FAP]<sup>-</sup> > [NCyF]<sup>-</sup> > [NPf<sub>2</sub>]<sup>-</sup>. Overall, this trend of  $\sigma$  for the [Pyrr<sub>14</sub>]<sup>+</sup>-based ILs is similar to that for 1-butyl-3-methylimidazolium-based ILs and 1-ethyl-3-methylimidazolium-based ILs.

**4.1.4 Surface Tension  $\gamma$ :** The values of  $\gamma$  of the target nonaromatic cation based ILs are listed in Table 2. As far as we know, the  $\gamma$  data of only about a half of the present ILs are reported.<sup>61,67,93,94,96,97,102,106,108,118,126,129,132</sup> The  $\gamma$  values of the remaining ILs are reported here, for the first time.

Figure 8 shows the  $\gamma$  value as a function of the number of carbons of the alkyl group in the cations of the [Pyrr<sub>1*n*][NTf<sub>2</sub>] series. For comparison, the data of the [C<sub>*n*</sub>MIm][NTf<sub>2</sub>] series are also given.<sup>59</sup> The data of the [Pyrr<sub>1*n*][NTf<sub>2</sub>] series fitted an exponential function:</sub></sub>

$$\gamma \text{ (mN/m)} = 28.3 \exp(-N_{RC} / 1.48) + 31.6 \quad (18)$$

In the case of the [Pyrr<sub>1*n*][NTf<sub>2</sub>] series, the relationship is given by  $\gamma \text{ (mN/m)} = 27.5 \exp(-N_{RC}/1.38) + 30.6$ , as shown in Figure 8. It is clear from Figure 8 that the change in  $\gamma$  to  $N_{RC}$  for the pyrrolidinium-based ILs is quite similar to that for the imidazolium-based ILs. However, the saturated  $\gamma$  value to  $N_{RC}$  in the pyrrolidinium-based ILs (31.6 mN/m) is slightly higher than that in the imidazolium-based ILs (30.6 mN/m). This implies that the surface of the IL is more structured (covered with alkyl groups) in the imidazolium-based ILs than in the pyrrolidinium-based ILs. The X-ray scattering study by Russina et al. showed that the nonaromatic piperidinium-based ILs are less segregated than their comparable imidazolium-based ILs.<sup>28</sup> Using sum frequency generation spectroscopy that is a surface-selective vibrational spectroscopy, looser or more defective structure of alkyl groups of cations in ammonium- and pyrrolidinium-based ILs than imidazolium-based ILs<sup>144</sup> was also observed.<sup>145</sup> The higher surface tension in the pyrrolidinium-based ILs than the respective imidazolium-based ILs is likely related to a similarly weak segregation or defective structure in the former ILs compared to the latter ILs.</sub>

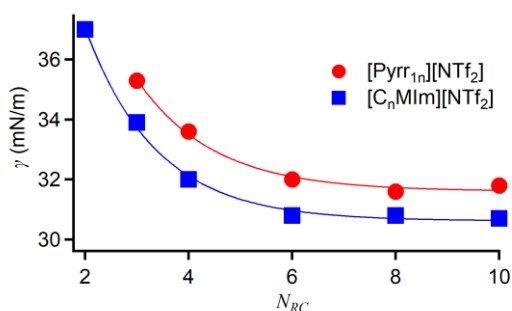


**Figure 8.** Plots of  $\gamma$  vs.  $N_{RC}$  for [Pyrr<sub>1*n*][NTf<sub>2</sub>] (red circles) and [C<sub>*n*</sub>MIm][NTf<sub>2</sub>] (blue squares).<sup>59</sup> Exponential fit functions are also shown by the respective colored lines.</sub>

On comparing the  $\gamma$  values of the pyrrolidinium- and piperidinium-based ILs, it was evident that the surface tension of the former ILs was slightly *lower* than that of the respective piperidinium-based ILs: 35.3 mN/m for [Pyrr<sub>13</sub>][NTf<sub>2</sub>] vs. 35.8 mN/m for [Pip<sub>13</sub>][NTf<sub>2</sub>], and 33.6 mN/m for [Pyrr<sub>14</sub>][NTf<sub>2</sub>] vs. 34.2 mN/m for [Pip<sub>14</sub>][NTf<sub>2</sub>]. The  $\gamma$  values of the ammonium- and phosphonium-based ILs ([N<sub>1444</sub>][NTf<sub>2</sub>] vs. [P<sub>1444</sub>][NTf<sub>2</sub>] and [N<sub>2228</sub>][NTf<sub>2</sub>] vs. [P<sub>2228</sub>][NTf<sub>2</sub>]) were similar. The substitution of an alkyl group with its respective alkoxyalkyl group (C<sub>4</sub>H<sub>9</sub>- → CH<sub>3</sub>OCH<sub>2</sub>CH<sub>2</sub>-) gave a slightly higher  $\gamma$

value. For example, the  $\gamma$  values of [Pyrr<sub>14</sub>][NTf<sub>2</sub>] and [Pyrr<sub>1(102)</sub>][NTf<sub>2</sub>] were 33.6 and 35.9 mN/m, respectively (Table 2).

From Table 2, the decreasing order of  $\gamma$  with respect to the different anions for the [Pyrr<sub>14</sub>]<sup>+</sup>-based ILs was found to be: [DCA]<sup>-</sup> > [TCM]<sup>-</sup> > [NF<sub>2</sub>]<sup>-</sup> > [OTf]<sup>-</sup> > [NCyF]<sup>-</sup> > [FAP]<sup>-</sup> ~ [NTf<sub>2</sub>]<sup>-</sup> > [NPf<sub>2</sub>]<sup>-</sup>.

Maroncelli and coworkers have reported a correlation between  $\gamma$  and  $V_m$  in molten salts including ILs.<sup>108</sup> Subsequently, a similar correlation between  $\gamma$  and  $V_m$  was identified in aromatic cation based ILs.<sup>59</sup> In the latter study, a dramatic change in  $V_m$  was observed in the low- $V_m$  region. Figure 9 displays the plots of  $\gamma$  vs.  $V_m$  for the present forty nonaromatic cation based ILs. The data for previously reported forty aromatic cation based ILs are also shown in the plots. The correlation between  $\gamma$  and  $V_m$  in the nonaromatic cation based ILs was slightly different from that in the case of aromatic cation based ILs. Similar to the reported data on the aromatic cation based ILs, the correlation for the nonaromatic cation based ILs was expressed by a single exponential function:

$$\gamma \text{ (mN/m)} = 265.1 \exp(-0.0123V_m) + 29.4 \quad (19)$$

Compared to the correlation for the aromatic cation based ILs ( $\gamma \text{ (mN/m)} = 178.5 \exp(-0.0124V_m) + 28.7$ ),<sup>59</sup> the parameters of the amplitudes of the exponential terms of the two types of ILs were different. This indicated that the intrinsic surface tension, which is defined as the value at zero molar volume, of the nonaromatic cation based ILs was higher than that of the aromatic cation based ILs.

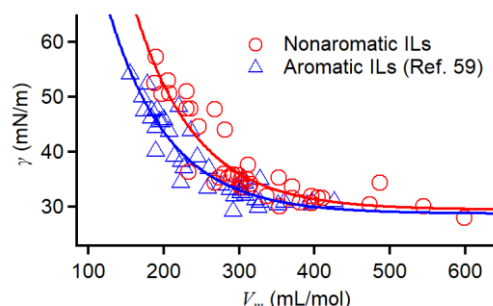


**Figure 9.** Plots of  $\gamma$  vs.  $V_m$  for the present forty nonaromatic cation based ILs (red circles) and forty aromatic cation based ILs (blue triangles).<sup>59</sup> Exponential fits are shown by corresponding colored lines.

## 4.2 Ultrafast Dynamics: Low-Frequency Spectra

### 4.2.1 General Features of Nonaromatic Cation Based

**ILs:** The intensity of the low-frequency spectrum in liquids and solutions obtained by fs-RIKES with the polarization configuration for the depolarized signal (like this study) depends on the magnitude of the collective polarizability anisotropy of the sample.<sup>7,146</sup> The molecular polarizability anisotropy of an aromatic molecule is usually larger than that of the corresponding nonaromatic molecule.<sup>147,148</sup> This is also true for ILs.<sup>34,44,60</sup> Therefore, the line shape in the low-frequency spectra of aromatic cation based ILs, such as imidazolium- and pyridinium-based ILs, is governed by the aromatic group. In fact, this makes difficult to understand the effect of the anion, whose magnitude of polarizability anisotropy is small, and thus its effect on the line shape of the spectrum, is relatively small as compared to that of typical aromatic cations.

Figure 10 compares the low-frequency Kerr spectra of the bis(fluorosulfonyl)amide salts of

1-butyl-1-methylpyrrolidinium ([Pyrr<sub>14</sub>][NF<sub>2</sub>]) and 1-butyl-3-methylimidazolium ([C<sub>4</sub>MIm][NF<sub>2</sub>]) cations, as an example. The spectral intensity relative to the electronic response of [Pyrr<sub>14</sub>][NF<sub>2</sub>] is smaller than that of [C<sub>4</sub>MIm][NF<sub>2</sub>]. According to the quantum chemistry calculations based on the B3LYP/6-311+G(3df) level of theory,<sup>60</sup> the polarizability anisotropy  $\alpha_{\text{anis}}$  of [Pyrr<sub>14</sub>]<sup>+</sup> was about half of that of [C<sub>4</sub>MIm]<sup>+</sup>. In this study, we also confirm that the results of the quantum chemistry calculations based on the B3LYP/6-311+G(d,p) level of theory show similar difference in  $\alpha_{\text{anis}}$  of the two cations ( $\alpha_{\text{anis}}([\text{Pyrr}_{14}]^+) = 3.515 \text{ \AA}^3$  and  $\alpha_{\text{anis}}([\text{C}_4\text{MIm}]^+) = 7.317 \text{ \AA}^3$  (Table S2-4 of the Electronic Supporting Information). This is consistent with the results in this study shown in Figure 10. This feature in the spectral density is rather general for the low-frequency spectra of other aromatic and nonaromatic cation based ILs, as well.<sup>34,60</sup>

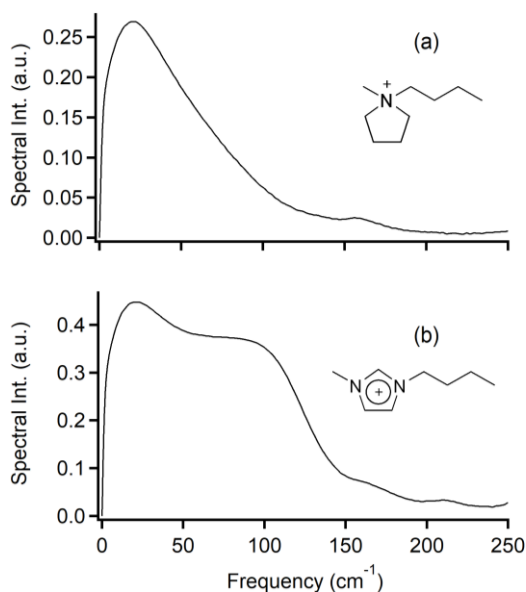


**Figure 10.** Comparison of the low-frequency Kerr spectra of (a) [Pyrr<sub>14</sub>][NF<sub>2</sub>] and (b) [C<sub>4</sub>MIm][NF<sub>2</sub>]. The spectrum of [C<sub>4</sub>MIm][NF<sub>2</sub>] was previously reported in Ref. 59.

There is a clear difference in the spectral line shapes between [Pyrr<sub>14</sub>][NF<sub>2</sub>] and [C<sub>4</sub>MIm][NF<sub>2</sub>], as shown in Figure 10. The line shape of the low-frequency Kerr spectrum of [Pyrr<sub>14</sub>][NF<sub>2</sub>] is triangular, while that of [C<sub>4</sub>MIm][NF<sub>2</sub>] is bimodal. The stronger spectral density in the high-frequency region above  $\sim 50 \text{ cm}^{-1}$  in aromatic cation based ILs, such as imidazolium- and pyridinium-based ILs,<sup>34,44</sup> compared to the nonaromatic cation based ILs with the same anions, is attributed to the libration of an aromatic ring. In fact, a substantial contribution of the aromatic ring libration to the low-frequency Kerr spectrum is observed not only for aromatic cation based ILs but also in aromatic molecular liquids. On comparing the low-frequency spectra of [Pyrr<sub>14</sub>][NF<sub>2</sub>] and [C<sub>4</sub>MIm][NF<sub>2</sub>], as shown in Figure 10, it was evident that the spectral line shape having the low-frequency peak at  $\sim 20 \text{ cm}^{-1}$  was mainly due to the anion [NF<sub>2</sub>]<sup>-</sup>. Accordingly, the line shape of the low-frequency spectrum of nonaromatic cation based ILs is useful to clarify the effects of the anion species on the spectrum line shape. In the following discussion, examples of low-frequency Kerr spectra are given for the forty nonaromatic cation based ILs with different cations and anions.

**4.2.2 Effect of Anion Species:** The effect of the anion species on the low-frequency Kerr spectrum of ILs is focused

in this section. As discussed in section 4.2.1, the contribution of the nonaromatic cation to the spectral density in the low-frequency broadened spectrum of the IL is small as compared to that of the aromatic cation. Therefore, the contribution of the anion species to the spectral line shape is often buried under the spectrum arising from the cation species. Consequently, it is useful to measure the low-frequency spectra of nonaromatic cation based ILs with a wide variety of anion species to understand their effects on the spectral line shape of the low-frequency Kerr spectrum of ILs.

Figure 11 compares the low-frequency spectra of ILs with spherical top anions, [PF<sub>6</sub>]<sup>-</sup> and [BF<sub>4</sub>]<sup>-</sup>. The spectral density mainly arises from the cations because of zero polarizability anisotropy of these anions ([PF<sub>6</sub>]<sup>-</sup>: *O<sub>h</sub>* and [BF<sub>4</sub>]<sup>-</sup>: *T<sub>d</sub>*). Thus, the spectral line shapes of the ILs with the spherical top anions are largely attributable to the cations. It is evident from Figure 11 that the line shapes of the low-frequency spectra of the three [BF<sub>4</sub>]<sup>-</sup> salts ([P<sub>444(2S2)</sub>][BF<sub>4</sub>] in particular) are different.

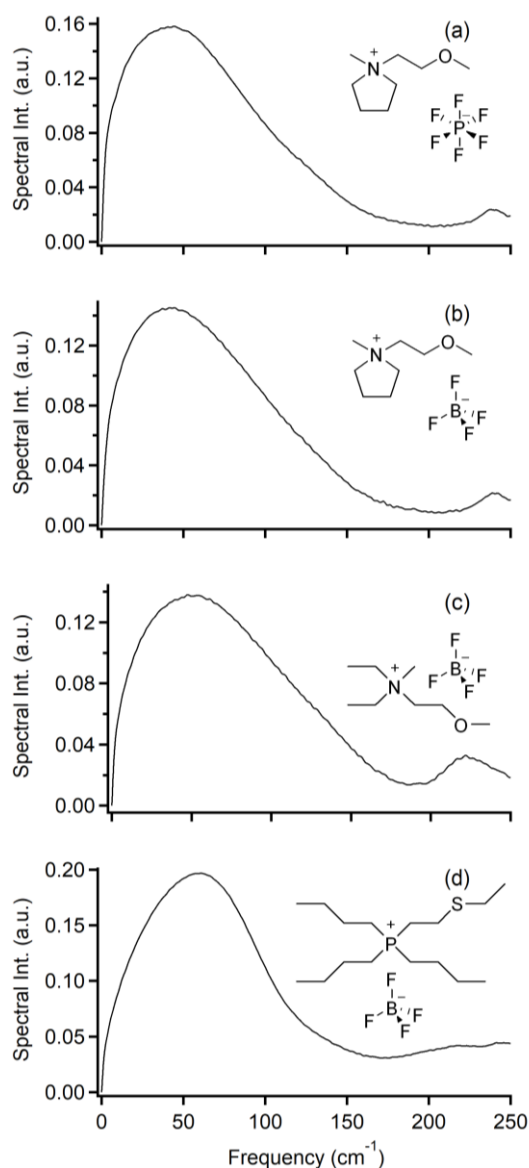


**Figure 11.** Low-frequency Kerr spectra of ILs with spherical top anions. (a) [Pyrr<sub>1(102)</sub>][PF<sub>6</sub>], (b) [Pyrr<sub>1(102)</sub>][BF<sub>4</sub>], (c) [N<sub>122(102)</sub>][BF<sub>4</sub>], and (d) [P<sub>444(2S2)</sub>][BF<sub>4</sub>].

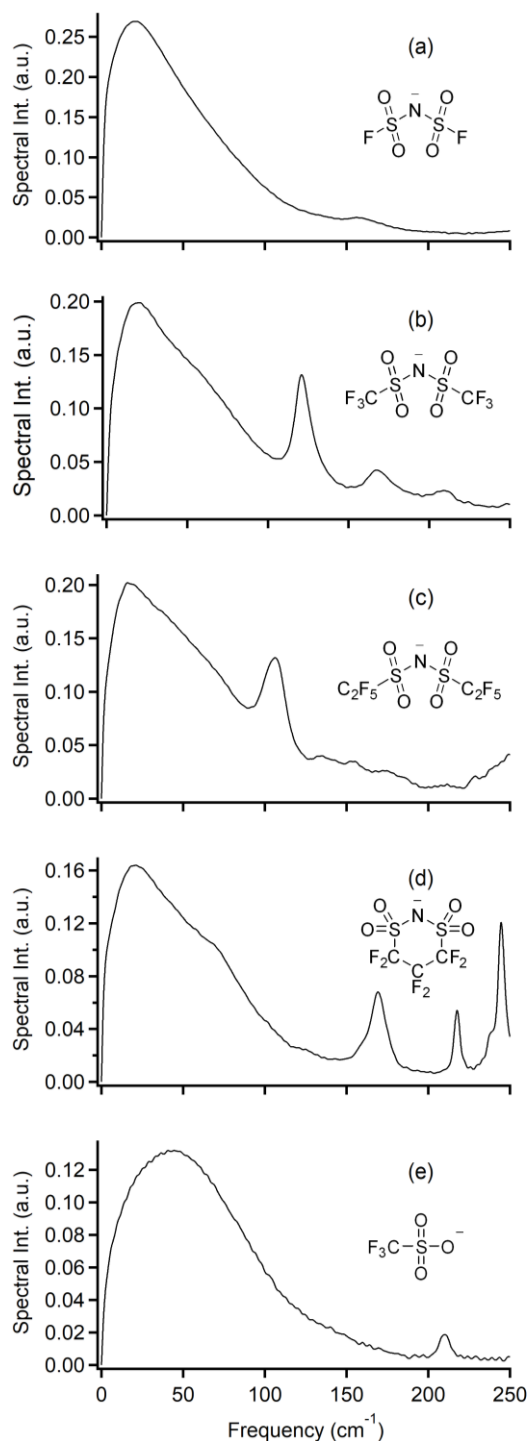
The line shapes of the low-frequency spectra of  $[\text{Pyrr}_{1(102)}][\text{PF}_6]$  and  $[\text{Pyrr}_{1(102)}][\text{BF}_4]$  are similar. However, the spectral intensity in the high-frequency region above  $\sim 70 \text{ cm}^{-1}$  for  $[\text{Pyrr}_{1(102)}][\text{BF}_4]$  is slightly higher than that for  $[\text{Pyrr}_{1(102)}][\text{PF}_6]$  (the spectral intensity at  $100 \text{ cm}^{-1}$  for  $[\text{Pyrr}_{1(102)}][\text{BF}_4]$  was  $\sim 0.6$  relative to the maximum intensity at  $\sim 50 \text{ cm}^{-1}$  and that for  $[\text{Pyrr}_{1(102)}][\text{PF}_6]$  was  $\sim 0.5$ ). The difference in the low-frequency spectra of  $[\text{Pyrr}_{1(102)}][\text{PF}_6]$  and  $[\text{Pyrr}_{1(102)}][\text{BF}_4]$  was similarly observed in the 1-butyl-3-methylimidazolium-based ILs with  $[\text{PF}_6]^-$  and  $[\text{BF}_4]^-$ .<sup>59</sup> Therefore, the origin of this type of difference in the spectra of the salts of  $[\text{PF}_6]^-$  and  $[\text{BF}_4]^-$  is the nature of the anions. As the molar volume and mean polarizability of  $[\text{PF}_6]^-$  are larger than those of  $[\text{BF}_4]^-$ , the collision-induced (or interaction-induced) intermolecular vibrational motion of  $[\text{PF}_6]^-$  likely contributed more strongly to the spectral density than  $[\text{BF}_4]^-$ , as observed by the higher spectral intensity in  $[\text{Pyrr}_{1(102)}][\text{PF}_6]$  than  $[\text{Pyrr}_{1(102)}][\text{BF}_4]$  (Figure 11).

Figure 12 shows the low-frequency spectra of  $[\text{Pyrr}_{14}]^+$ -based ILs with  $[\text{NF}_2]^-$ ,  $[\text{NTf}_2]^-$ ,  $[\text{NPF}_2]^-$ ,  $[\text{NCyF}]^-$ , and  $[\text{OTf}]^-$ . When we compare the spectra of the ILs with the anions of bis(perfluoroalkylsulfonyl)amide derivatives,  $[\text{NF}_2]^-$ ,  $[\text{NTf}_2]^-$ , and  $[\text{NPF}_2]^-$ , triangular spectral line shapes are observed. The peak shifts to lower frequencies in the order of  $[\text{Pyrr}_{14}][\text{NF}_2]$  ( $\sim 21 \text{ cm}^{-1}$ )  $>$   $[\text{Pyrr}_{14}][\text{NTf}_2]$  ( $\sim 20 \text{ cm}^{-1}$ )  $>$   $[\text{Pyrr}_{14}][\text{NPF}_2]$  ( $\sim 18 \text{ cm}^{-1}$ ). This order is also valid for the spectral peak in the low-frequency region below  $30 \text{ cm}^{-1}$  in the tributyldecylphosphonium-based ILs, although the peak is a little ambiguous for the spectral density of the cation (Figure S1 of the Electronic Supporting Information). Previously, we assigned the peak for imidazolium-based ILs with these anions to the anion species, and the trend for the ILs was the same as the results of  $[\text{Pyrr}_{14}]^+$ -based ILs.<sup>149</sup> This order is trivial, because the order of the peak frequencies of the three ILs is the inverse of the trend of the volumes and masses of the anion species. In addition to the order of the peak frequencies, the spectral intensity in the higher frequency region above  $\sim 50 \text{ cm}^{-1}$  increased in the order of  $[\text{Pyrr}_{14}][\text{NF}_2] < [\text{Pyrr}_{14}][\text{NTf}_2] < [\text{Pyrr}_{14}][\text{NPF}_2]$ .

The line shape of the low-frequency spectrum of  $[\text{Pyrr}_{14}][\text{OTf}]$  is quite different from those of  $[\text{Pyrr}_{14}][\text{NF}_2]$ ,  $[\text{Pyrr}_{14}][\text{NTf}_2]$ , and  $[\text{Pyrr}_{14}][\text{NPF}_2]$ ; rather, it is closer to that of  $[\text{Pyrr}_{1(102)}][\text{PF}_6]$ ,  $[\text{Pyrr}_{1(102)}][\text{BF}_4]$ , and  $[\text{N}_{122(102)}][\text{BF}_4]$  (Figure 11). In fact, the polarizability anisotropy of  $[\text{OTf}]^-$  is almost null ( $\alpha_{\text{anis}}([\text{OTf}]^-) = 0.327 \text{ \AA}^3$ , Table S2-4 of the Electronic Supporting Information). On the other hand, the other anions possess the substantial magnitudes of the polarizability anisotropy ( $\alpha_{\text{anis}}([\text{NF}_2]^-) = 3.396 \text{ \AA}^3$ ,  $\alpha_{\text{anis}}([\text{NTf}_2]^-) = 3.942 \text{ \AA}^3$ , and  $\alpha_{\text{anis}}([\text{NPF}_2]^-) = 6.052 \text{ \AA}^3$ , Table S2-4 of the Electronic Supporting Information). Thus, the distinct line shape of the low-frequency spectrum of  $[\text{Pyrr}_{14}][\text{OTf}]$  compared to  $[\text{Pyrr}_{14}][\text{NF}_2]$ ,  $[\text{Pyrr}_{14}][\text{NTf}_2]$ , and  $[\text{Pyrr}_{14}][\text{NPF}_2]$  is attributed to the polarizability anisotropy of the anion.

The line shape of the low-frequency Kerr spectrum of  $[\text{Pyrr}_{14}][\text{NCyF}]$  is triangular and similar to those of  $[\text{Pyrr}_{14}][\text{NF}_2]$ ,  $[\text{Pyrr}_{14}][\text{NTf}_2]$ , and  $[\text{Pyrr}_{14}][\text{NPF}_2]$ , as shown in Figure 12.  $[\text{NCyF}]^-$  possesses a similar structure and polarizability anisotropy value ( $\alpha_{\text{anis}}([\text{NCyF}]^-) = 2.694 \text{ \AA}^3$ , Table S2-4 of the Electronic Supporting Information) as  $[\text{NF}_2]^-$ ,  $[\text{NTf}_2]^-$ , and  $[\text{NPF}_2]^-$ .

Figure 13 shows the calculated Raman spectra of  $[\text{NF}_2]^-$ ,  $[\text{NTf}_2]^-$ ,  $[\text{NPF}_2]^-$ ,  $[\text{NCyF}]^-$ , and  $[\text{OTf}]^-$ . The strong Raman bands at  $104 \text{ cm}^{-1}$  for  $[\text{NTf}_2]^-$  and at  $95 \text{ cm}^{-1}$  for  $[\text{NPF}_2]^-$  are the coupled bending modes (symmetric N–S–C bending motions). The strong bands at  $120 \text{ cm}^{-1}$  observed in the Kerr spectrum of  $[\text{Pyrr}_{14}][\text{NTf}_2]$  and  $106 \text{ cm}^{-1}$  for  $[\text{Pyrr}_{14}][\text{NPF}_2]$  shown in Figure



**Figure 12.** Low-frequency Kerr spectra of (a)  $[\text{Pyrr}_{14}][\text{NF}_2]$ , (b)  $[\text{Pyrr}_{14}][\text{NTf}_2]$ , (c)  $[\text{Pyrr}_{14}][\text{NPF}_2]$ , (d)  $[\text{Pyrr}_{14}][\text{NCyF}]$ , and (e)  $[\text{Pyrr}_{14}][\text{OTf}]$ .

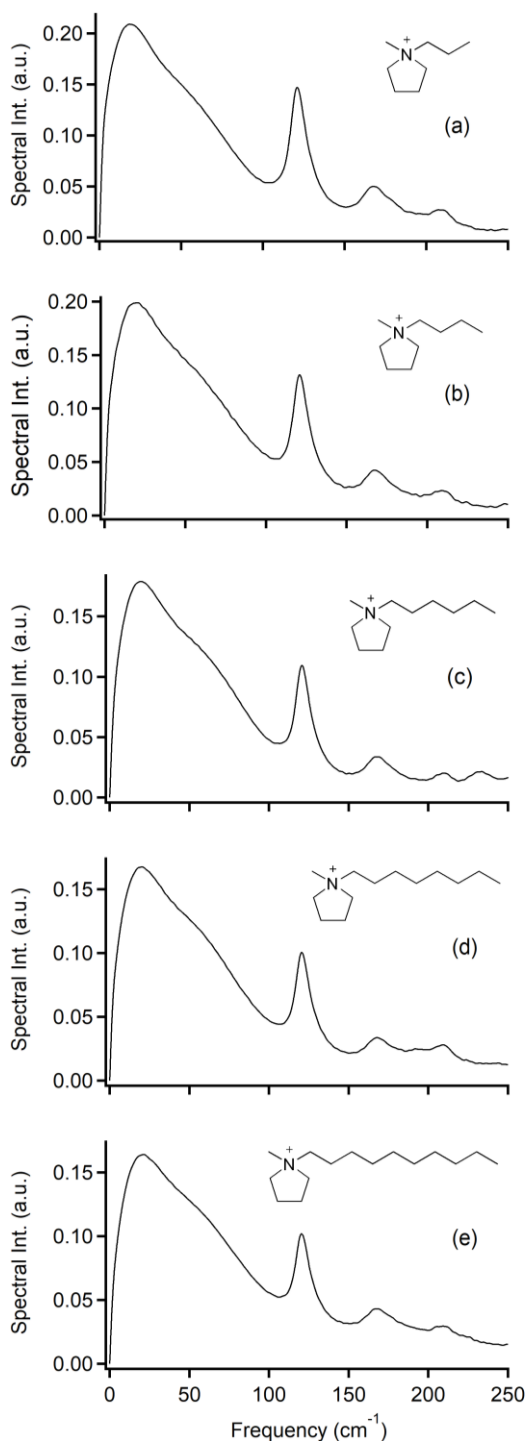
12 are assigned to the modes of the anion species. The quantum chemistry calculations also show no strong Raman-active modes in the low-frequency region below  $70 \text{ cm}^{-1}$ . Thus, the differences in the low-frequency broadened spectra of  $[\text{Pyrr}_{14}][\text{NF}_2]$ ,  $[\text{Pyrr}_{14}][\text{NTf}_2]$ ,  $[\text{Pyrr}_{14}][\text{NPF}_2]$ ,  $[\text{Pyrr}_{14}][\text{NCyF}]$ , and  $[\text{Pyrr}_{14}][\text{OTf}]$  shown in Figure 12 arise primarily from the difference in the intermolecular vibrations of the anion species.

The line shape of the low-frequency spectrum of  $[\text{Pyrr}_{14}][\text{NCyF}]$  is similar to that of  $[\text{Pyrr}_{14}][\text{NTf}_2]$  and  $[\text{Pyrr}_{14}][\text{NPF}_2]$ . On the other hand, the spectral shape for



many bands above  $100\text{ cm}^{-1}$  in the Kerr spectrum are essentially attributable to the intramolecular vibrational bands of  $[\text{FAP}]^-$ .

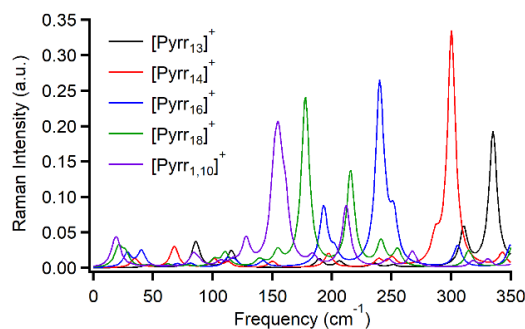
**4.2.3 Effects of Cation Species:** We examine the effect of the cation species on the low-frequency Kerr spectrum in this section. Compared to the anion species, the contribution of the cation species to the low-frequency Kerr spectrum in ILs is not large. However, it is also important to understand the effect of the cations on the low-frequency Kerr spectrum in detail.



**Figure 16.** Low-frequency Kerr spectra of the  $[\text{Pyrr}_{1n}][\text{NTf}_2]$  series. (a)  $[\text{Pyrr}_{13}][\text{NTf}_2]$ , (b)  $[\text{Pyrr}_{14}][\text{NTf}_2]$ , (c)  $[\text{Pyrr}_{16}][\text{NTf}_2]$ , (d)  $[\text{Pyrr}_{18}][\text{NTf}_2]$ , and (e)  $[\text{Pyrr}_{1,10}][\text{NTf}_2]$ .

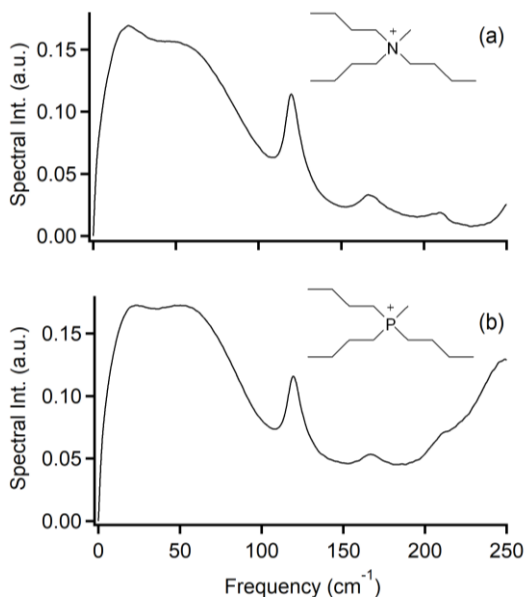
Figure 16 shows the low-frequency Kerr spectra of the  $[\text{Pyrr}_{1n}][\text{NTf}_2]$  series. Though there are small differences in the spectral shapes in the frequency range from  $150$  to  $250\text{ cm}^{-1}$  of the  $[\text{Pyrr}_{1n}][\text{NTf}_2]$  series probably owing to the intramolecular vibrational modes of the alkyl groups, the line shapes of the low-frequency broadened bands in the frequency below  $100\text{ cm}^{-1}$  are quite similar. This spectral feature in the  $[\text{Pyrr}_{1n}][\text{NTf}_2]$  series is in contrast to the  $[\text{C}_n\text{MIm}][\text{NTf}_2]$  series. The difference in the line shapes of the low-frequency spectra of the  $[\text{C}_n\text{MIm}][\text{NTf}_2]$  series was attributed to the bending mode between the imidazolium ring and alkyl group, which shifts to lower frequencies for ILs with longer (heavier) alkyl groups.<sup>59</sup>

Calculated Raman spectra of the  $[\text{Pyrr}_{1n}]^+$  based on the ab initio quantum chemistry calculations are shown in Figure 17. A significant alkyl group substitution effect is confirmed in the bend and torsion coupled with the pyrrolidinium ring torsion:  $335\text{ cm}^{-1}$  for  $[\text{Pyrr}_{13}]^+$ ,  $300\text{ cm}^{-1}$  for  $[\text{Pyrr}_{14}]^+$ ,  $240\text{ cm}^{-1}$  for  $[\text{Pyrr}_{16}]^+$ ,  $178\text{ cm}^{-1}$  for  $[\text{Pyrr}_{18}]^+$ , and  $155\text{ cm}^{-1}$  for  $[\text{Pyrr}_{1,10}]^+$ . On the other hand, the Raman intensities of the low-frequency modes below  $100\text{ cm}^{-1}$  of  $[\text{Pyrr}_{1n}]^+$  are very weak. Therefore, it is concluded that the intramolecular band does not influence the line shape of the low-frequency spectrum. Consequently, the line shapes of the low-frequency Kerr spectra of the five  $[\text{Pyrr}_{1n}][\text{NTf}_2]$  are quite similar (Figure 16).



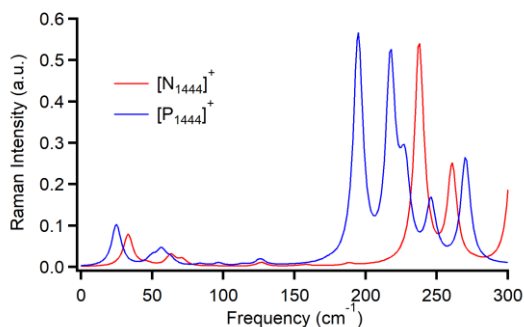
**Figure 17.** Calculated Raman spectra of  $[\text{Pyrr}_{13}]^+$  (black line),  $[\text{Pyrr}_{14}]^+$  (red line),  $[\text{Pyrr}_{16}]^+$  (blue line),  $[\text{Pyrr}_{18}]^+$  (green line), and  $[\text{Pyrr}_{1,10}]^+$  (purple line) optimized at the B3LYP/6-311+G(d,p) level of theory.

Figure 18 compares the low-frequency Kerr spectra of the ammonium- and phosphonium-based ILs,  $[\text{N}_{1444}][\text{NTf}_2]$  and  $[\text{P}_{1444}][\text{NTf}_2]$ . The spectral intensity at  $\sim 50\text{ cm}^{-1}$  relative to that at  $\sim 20\text{ cm}^{-1}$  is slightly higher in  $[\text{P}_{1444}][\text{NTf}_2]$  as compared to  $[\text{N}_{1444}][\text{NTf}_2]$ . Such a spectral feature was also observed in  $[\text{N}_{2228}][\text{NTf}_2]$  and  $[\text{P}_{2228}][\text{NTf}_2]$ <sup>61</sup> (also see the Electronic Supporting Information). Because the phosphonium cations show stronger intramolecular vibrational bands in the frequency range above  $150\text{ cm}^{-1}$  than the ammonium cations, the spectral wing at the low-frequency side of the intramolecular vibrational bands likely contribute to the higher relative intensity at  $\sim 50\text{ cm}^{-1}$  in the phosphonium-based ILs as compared to the ammonium-based ILs. Compared to the calculated Raman spectra of  $[\text{N}_{1444}]^+$  and  $[\text{P}_{1444}]^+$  by the quantum chemistry calculations based on the B3LYP/6-311+G(d,p) level of theory shown in Figure 19, one can think that the stronger spectral intensity in the frequency region  $50 - 100\text{ cm}^{-1}$  of the low-frequency Kerr spectrum of  $[\text{P}_{1444}][\text{NTf}_2]$  than that of  $[\text{N}_{1444}][\text{NTf}_2]$  might be attributed to the lower frequencies of the torsional motions of the butyl groups in  $[\text{P}_{1444}]^+$  than  $[\text{N}_{1444}]^+$  (note that bands in the frequency of  $170 - 300\text{ cm}^{-1}$  in Figure 19 are only the most stable conformation in each cation).



**Figure 18.** Comparison of low-frequency Kerr spectra of ammonium- and phosphonium-based ILs. (a)  $[N_{1444}][NTf_2]$  and (b)  $[P_{1444}][NTf_2]$ .

The low-frequency Kerr spectra of  $[Pyrr_{14}][NF_2]$  and  $[Pyrr_{1(102)}][NF_2]$  are shown in Figure 20 and illustrate the effect of substituting an alkyl group with its respective alkoxyalkyl group. The spectral line shapes of the two ILs are quite similar, as shown in Figure 20. A small difference in the low-frequency spectra between the two ILs is confirmed in the frequency range of  $\sim 80\text{--}150\text{ cm}^{-1}$ .  $[Pyrr_{1(102)}][NF_2]$  shows a slightly higher spectral intensity in this frequency region than  $[Pyrr_{14}][NF_2]$ . Other ILs with butyl and methoxyethyl groups in this study also show similar spectral line shapes. This spectral feature was also confirmed in  $[Pyrr_{14}][NTf_2]$  and  $[Pyrr_{1(102)}][NTf_2]$ . As seen in the spectra of the Raman-active normal modes of  $[Pyrr_{14}]^+$  and  $[Pyrr_{1(102)}]^+$  based on the B3LYP/6-311+G(d,p) level of theory of Figure 21,  $[Pyrr_{1(102)}]^+$  has a weak intramolecular mode at  $\sim 140\text{ cm}^{-1}$  that is the torsional mode of the pyrrolidinium ring coupled with the bending motion of the methoxyethyl group and pyrrolidinium ring. This vibrational band can influence the slight difference in the frequency region of  $\sim 80\text{--}150\text{ cm}^{-1}$ . In addition, we found a weak intramolecular vibrational band at  $\sim 240\text{ cm}^{-1}$  of  $[Pyrr_{1(102)}]^+$ , which is not observed in  $[Pyrr_{14}]^+$ . A weak



**Figure 19.** Calculated Raman spectra of  $[N_{1444}]^+$  (red line) and  $[P_{1444}]^+$  (blue line) optimized at the B3LYP/6-311+G(d,p) level of theory.

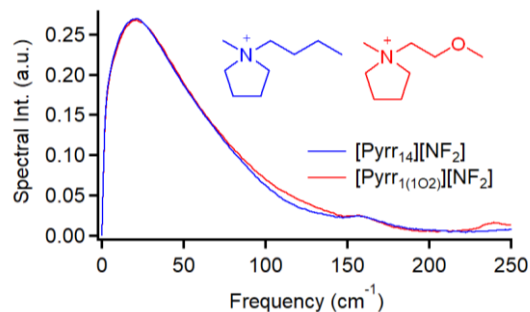


**Figure 20.** Low-frequency Kerr spectra of  $[Pyrr_{14}][NF_2]$  (blue) and  $[Pyrr_{1(102)}][NF_2]$  (red).

intramolecular Raman-active band is also observed for the optimized  $[Pyrr_{1(102)}]^+$  at  $\sim 250\text{ cm}^{-1}$  (see Figure 21). The vibrational band at  $\sim 240\text{ cm}^{-1}$  of  $[Pyrr_{1(102)}]^+$  is hard to confirm in the ILs with more complicated anions, but the ILs with simpler anions ( $[BF_4]^-$  and  $[PF_6]^-$ ) also show this band (Figure S1 of the Electronic Supporting Information).

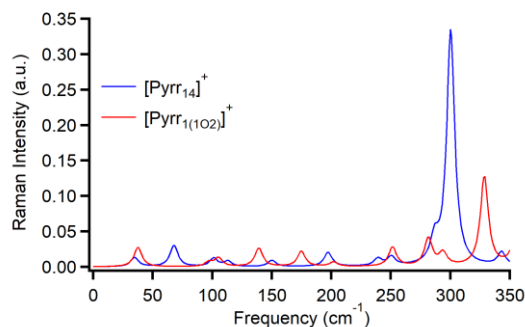


**Figure 21.** Calculated Raman spectra of  $[Pyrr_{14}]^+$  (blue line) and  $[Pyrr_{1(102)}]^+$  (red line) optimized at the B3LYP/6-311+G(d,p) level of theory.

### 4.3 Relationship between Low-Frequency Spectrum and Bulk Parameter

Previously, we have reported that there is a linear relationship between  $M_1$  and  $(\gamma/\rho)^{1/2}$  for forty aprotic molecular liquids.<sup>13</sup> The idea of this type of plots is based on a simple consideration that the intermolecular vibrational band regards as the harmonic oscillator. The vibrational frequency of the harmonic oscillator  $\tilde{\nu}$  is given as

$$\tilde{\nu} = \frac{1}{2\pi c} \sqrt{\frac{k}{\mu}} \quad (20)$$

where  $c$  is the velocity of light,  $k$  is the force constant, and  $\mu$  is the reduced mass. For the intermolecular vibrational band, Eq. (20) can be rewritten as

$$M_1 \propto \sqrt{\frac{\gamma}{\rho}} \quad (21)$$

The constants  $k$  and  $\mu$  in the harmonic oscillator correspond to  $\gamma$  and  $\rho$  in the intermolecular vibration, respectively. It should be noted that  $k$  and  $\mu$  are the parameters of the oscillator itself (intramolecular parameters), but  $\gamma$  and  $\rho$  are the bulk parameters. In a sense, Eq. (21) implies a sort of scaling relation between the microscopic (intermolecular vibration) and macroscopic (bulk liquid properties) quantities. A linear relation between  $M_1$  and  $(\gamma/\rho)^{1/2}$  was also observed in aromatic cation based ILs, although it is different from that for aprotic

molecular liquids.<sup>59</sup>

Figure 22 plots the  $M_1$  values to the  $(\gamma/\rho)^{1/2}$  for the nonaromatic cation based ILs. As shown in the figure, there is a mild linear correlation between the two quantities, though the data are scattered compared to aprotic MLs. The figure also shows that the relation for the nonaromatic cation based ILs is close to that for aprotic molecular liquids, but clearly different from that for aromatic cation based ILs. The relations estimated by the linear fits together with their correlation parameters,  $r$ , are followings:

$$M_1(\text{cm}^{-1}) = 7.11(\pm 1.28)\sqrt{\gamma(\text{mN/m})/\rho(\text{g/mL})} + 14.5(\pm 7.0) \quad (r = 0.67) \quad \text{(nonaromatic cation based ILs)} \quad (22)$$

$$M_1(\text{cm}^{-1}) = 3.51(\pm 0.95)\sqrt{\gamma(\text{mN/m})/\rho(\text{g/mL})} + 48.6(\pm 5.2) \quad (r = 0.51) \quad \text{(aromatic cation based ILs)}^{59} \quad (23)$$

$$M_1(\text{cm}^{-1}) = 11.2(\pm 0.9)\sqrt{\gamma(\text{mN/m})/\rho(\text{g/mL})} - 9.12(\pm 5.1) \quad (r = 0.86) \quad \text{(aprotic MLs)}^{13,72,151} \quad (24)$$

It should be reminded that the relation for aprotic molecular liquids includes the data for both aromatic and nonaromatic MLs.

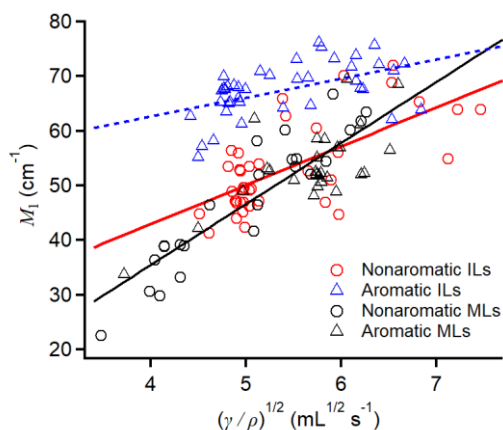


**Figure 22.** Plots of  $M_1$  versus  $(\gamma/\rho)^{1/2}$  for nonaromatic cation based ILs (red circles). Linear fit for the data is shown by a red solid line. Relationships between  $M_1$  and  $(\gamma/\rho)^{1/2}$  for aprotic MLs (nonaromatic MLs: black circles; aromatic MLs: black triangles)<sup>13,72,151</sup> and aromatic cation based ILs (blue triangles).<sup>59</sup>

In previous preliminary results, a less sensitive  $M_1$  to  $(\gamma/\rho)^{1/2}$  relation is found for the aromatic cation based ILs than aprotic MLs and nonaromatic cation based ILs (only ten nonaromatic cation based ILs in that study).<sup>34</sup> The weak bulk parameter dependence of  $M_1$  in aromatic cation based ILs as compared to that in aprotic MLs (and some nonaromatic cation based ILs) was mainly attributed to the spectral density and the more segregated structure in ILs.<sup>34</sup> This is because  $[\text{C}_n\text{MIm}][\text{NTf}_2]$  (aromatic cation based ILs) showed clearer low- $Q$  (low scattering vector) peaks at  $\sim 4 \text{ nm}^{-1}$  owing to micro segregation than 1-alkyl-1-methylpiperidinium bis(trifluoromethylsulfonyl)amides (nonaromatic cation based ILs).<sup>152</sup> On the basis of the data of these forty nonaromatic cation based ILs, it is clear that the relationships for the nonaromatic and aromatic cation based ILs are different in this study. It should be emphasized that aprotic MLs show a single linear correlation for both aromatic and nonaromatic MLs, but

the ILs show different relations for nonaromatic and aromatic ILs. In addition, the relation for nonaromatic ILs is close to that for aprotic MLs. This relation between  $M_1$  and  $(\gamma/\rho)^{1/2}$  in liquids seems to be universal, except for aromatic cation based ILs. However, slightly weaker  $(\gamma/\rho)^{1/2}$  dependence of  $M_1$  is observed for the nonaromatic cation based ILs than aprotic MLs. This might also be originated from the micro segregation structure in nonaromatic cation based ILs, though it is not significant when compared to that in aromatic cation based ILs. We therefore believe that the relation between  $M_1$  and  $(\gamma/\rho)^{1/2}$  in liquids is rather universal, although the segregation structure also influences the relation. Accordingly, liquids with no segregation structure likely obey this relationship between the microscopic and macroscopic quantities.

## 5. Conclusions

In this study, we reported the low-frequency spectral data of as many as forty nonaromatic cation based ILs via fs-RIKES, as well as the data of liquid properties,  $\rho$ ,  $\eta$ ,  $\sigma$ , and  $\gamma$ . On the basis of the data of liquid properties of  $[\text{Pyrr}_{14}]^+$ -based ILs, the following trends were identified:

density ( $\rho$ ),  $[\text{FAP}]^- > [\text{NPF}_2]^- > [\text{NCyF}]^- > [\text{NTf}_2]^- > [\text{NF}_2]^- > [\text{OTf}]^- > [\text{DCA}]^- \sim [\text{TCM}]^-$ ;

viscosity ( $\eta$ ),  $[\text{NCyF}]^- > [\text{NPF}_2]^- > [\text{FAP}]^- > [\text{OTf}]^- > [\text{NTf}_2]^- > [\text{NF}_2]^- > [\text{DCA}]^- > [\text{TCM}]^-$ ;

electrical conductivity ( $\sigma$ ),  $[\text{DCA}]^- > [\text{NF}_2]^- > [\text{TCM}]^- > [\text{NTf}_2]^- > [\text{OTf}]^- > [\text{FAP}]^- > [\text{NCyF}]^- > [\text{NPF}_2]^-$ ;

surface tension ( $\gamma$ ),  $[\text{DCA}]^- > [\text{TCM}]^- > [\text{NF}_2]^- > [\text{OTf}]^- > [\text{NCyF}]^- > [\text{FAP}]^- > [\text{NTf}_2]^- > [\text{NPF}_2]^-$ .

On the basis of the results of the  $[\text{Pyrr}_{1n}][\text{NTf}_2]$  series, the relationships between the liquid properties and the number of carbons of the alkyl groups for 1-alkyl-1-methylpyrrolidinium cations were also estimated. The plots of  $\sigma$  or  $A$  vs.  $\eta^{-1}$  for the nonaromatic cation based ILs showed a linear relationship, which was somewhat different from that of aromatic cation based ILs. In addition, the relationship between  $\gamma$  and  $V_m$  for nonaromatic cation based ILs, especially in the lower  $V_m$  region below  $\sim 300 \text{ mL/mol}$ , was different from that in the case of aromatic cation based ILs.

Further, the broad low-frequency Kerr spectra in the frequency below  $\sim 200 \text{ cm}^{-1}$  were discussed on the basis of the ion species. Compared to common aromatic cation based ILs, the intensity of the low-frequency spectrum of nonaromatic cation based ILs was quite low because of the absence of an aromatic ring, whose libration has a strong spectral intensity. However, ILs with a flat anion, such as dicyanamide and tricyanomethide, showed a relatively strong spectral density owing to the libration of the anions. From the comparison of the anions  $[\text{NF}_2]^-$ ,  $[\text{NTf}_2]^-$ , and  $[\text{NPF}_2]^-$  for  $[\text{Pyrr}_{14}]^+$ -based ILs and 1-(methoxy)ethyl-1-methylpyrrolidinium-based ILs, the peak at  $\sim 20 \text{ cm}^{-1}$  shifted to lower frequency with the increasing size of the anions:  $[\text{NF}_2]^- > [\text{NTf}_2]^- > [\text{NPF}_2]^-$ . The line shape of the low-frequency spectrum of  $[\text{Pyrr}_{1n}][\text{NTf}_2]$  was not sensitive to the alkyl group, unlike the  $[\text{C}_n\text{MIm}][\text{NTf}_2]$  and  $[\text{C}_n\text{Py}][\text{NTf}_2]$  series. From the results of the normal mode quantum chemistry calculations of 1-alkyl-1-methylpyrrolidinium cations, it was found that there was no intense Raman-active intramolecular vibrational band in the low-frequency region below  $\sim 100 \text{ cm}^{-1}$ , where the intermolecular vibrational band typically appears. The line shapes of the low-frequency Kerr spectra of ammonium-based ILs and the respective phosphonium-based ILs were significantly different. The difference could be largely attributed to the lower-frequency intramolecular vibrational bands of the phosphonium cation compared to the respective ammonium cation. The substitution of the butyl group of  $[\text{Pyrr}_{14}]^+$  by a methoxyethyl group did not influence the line

shape of the low-frequency spectrum of the ILs.

In addition, a linear relationship between the first moment  $M_1$  of the low-frequency spectrum and the bulk parameter,  $(\gamma/\rho)^{1/2}$ , was observed. Compared to our previous studies of aprotic MLs<sup>13</sup> and aromatic ILs,<sup>59</sup> this relationship for the nonaromatic cation based ILs was quite similar to that for aprotic MLs, including nonaromatic and aromatic analogs. However, it was different from that for aromatic cation based ILs. The distinct feature in the relation between  $M_1$  and  $(\gamma/\rho)^{1/2}$  for aromatic cation based ILs could be attributed to the significant segregation liquid structure in these ILs as compared to the nonaromatic cation based ILs, as well as aprotic MLs.

#### Acknowledgements

This work was partially supported by JSPS KAKENHI (15K05377 and 19K05382), the Takahashi Industrial and Economic Research Foundation, and Chiba University (Global Prominent Research Program: Soft Molecular Activation). S.K. was supported by JSPS Research Fellowship for Young Scientists (18J12979).

#### Electronic Supporting Information

Synthesis procedures of ILs, quantum chemistry calculation results, data of the Kerr transients and Fourier transform Kerr spectra, and lists of the fitting parameters for the Kerr transients and spectra of the nonaromatic cation based ILs are given in the Electronic Supporting Information.

#### References

- 1 A. Nitzan, *Chemical Dynamics in Condensed Phases. Relaxation, Transfer and Reactions in Condensed Molecular Systems.*, Editor, Oxford University Press, Oxford, **2006**.
- 2 A. M. Kelley, *Condensed-Phase Molecular Spectroscopy and Photophysics.* Editor, John Wiley & Sons, Inc., Hoboken, **2013**.
- 3 D. McMorrow, W. T. Lotshaw, G. A. Kenney-Wallace, *IEEE J. Quantum. Electron.* **1988**, *QE-24*, 443-454.
- 4 R. Righini, *Science* **1993**, *262*, 1386-1390.
- 5 C. A. Schmittenmaer, *Chem. Rev.* **2004**, *104*, 1759-1779.
- 6 J. B. Baxter, G. W. Guglietta, *Anal. Chem.* **2011**, *83*, 4342-4368.
- 7 W. T. Lotshaw, D. McMorrow, N. Thanttu, J. S. Melinger, R. Kitchenham, *J. Raman Spectrosc.* **1995**, *26*, 571-583.
- 8 S. Kinoshita, Y. Kai, T. Ariyoshi, Y. Shimada, *Inter. J. Mod. Phys. B* **1996**, *10*, 1229-1272.
- 9 E. W. Castner, Jr., M. Maroncelli, *J. Mol. Liq.* **1998**, *77*, 1-36.
- 10 J. T. Fourkas, in *Ultrafast Infrared and Raman Spectroscopy*, ed. by M. D. Fayer, Marcel Dekker, Inc., New York, **2001**, Chap. 11, pp. 473-512.
- 11 N. A. Smith, S. R. Meech, *Int. Rev. Phys. Chem.* **2002**, *21*, 75-100.
- 12 Q. Zhong, J. T. Fourkas, *J. Phys. Chem. B* **2008**, *112*, 15529-15539.
- 13 H. Shirota, T. Fujisawa, H. Fukazawa, K. Nishikawa, *Bull. Chem. Soc. Jpn.* **2009**, *82*, 1347-1366.
- 14 B. J. Loughnane, R. A. Farrer, A. Scodinu, T. Reilly, J. T. Fourkas, *J. Phys. Chem. B* **2000**, *104*, 5421-5429.
- 15 R. A. Farrer, J. T. Fourkas, *Acc. Chem. Res.* **2003**, *36*, 605-612.
- 16 N. T. Hunt, A. A. Jaye, S. R. Meech, *Phys. Chem. Chem. Phys.* **2007**, *9*, 2167-2180.
- 17 J. S. Wilkes, M. J. Zaworotko, *J. Chem. Soc., Chem. Commun.* **1992**, 965-967.
- 18 J. S. Wilkes, *Green Chem.* **2002**, *4*, 73-80.
- 19 P. Wasserscheid, T. Welton, *Ionic Liquids in Synthesis.* 2 ed., P. Wasserscheid, T. Welton, Wiley-VCH, Weinheim, **2008**.
- 20 H. Ohno, *Electrochemical Aspects of Ionic Liquids.* H. Ohno, Wiley-Interscience, Hoboken, **2005**.
- 21 J. A. Ingram, R. S. Moog, N. Ito, R. Biswas, M. Maroncelli, *J. Phys. Chem. B* **2003**, *107*, 5926-5932.
- 22 A. Samanta, *J. Phys. Chem. Lett.* **2010**, *1*, 1557-1562.
- 23 Y. Nagasawa, *J. Photochem. Photobiol. C: Photochem. Rev.* **2011**, *12*, 31-45.
- 24 Y. Murakami, H. Kikuchi, A. Kawai, *J. Phys. Chem. B* **2013**, *117*, 5180-5187.
- 25 K. Fujii, M. Aramaki, Y. Kimura, *J. Phys. Chem. B* **2018**, *122*, 12363-12374.
- 26 C. Hardacre, J. D. Holbrey, M. Nieuwenhuyzen, T. G. A. Youngs, *Acc. Chem. Res.* **2007**, *40*, 1146-1150.
- 27 E. W. Castner, Jr., C. J. Margulis, M. Maroncelli, J. F. Wishart, *Annu. Rev. Phys. Chem.* **2011**, *62*, 85-105.
- 28 O. Russina, A. Triolo, L. Gontrani, R. Caminiti, *J. Phys. Chem. Lett.* **2012**, *3*, 27-33.
- 29 J. C. Araque, J. J. Hettige, C. J. Margulis, *J. Phys. Chem. B* **2015**, *119*, 12727-12740.
- 30 E. W. Castner, Jr., J. F. Wishart, H. Shirota, *Acc. Chem. Res.* **2007**, *40*, 1217-1227.
- 31 K. Iwata, H. Okajima, S. Saha, H.-O. Hamaguchi, *Acc. Chem. Res.* **2007**, *40*, 1174-1181.
- 32 K. Fumino, S. Reimann, R. Ludwig, *Phys. Chem. Chem. Phys.* **2014**, *16*, 21903-21929.
- 33 V. H. Paschoal, L. F. O. Faria, M. C. C. Ribeiro, *Chem. Rev.* **2017**, *117*, 7053-7112.
- 34 H. Shirota, *ChemPhysChem* **2012**, *13*, 1638-1648.
- 35 H. Shirota, H. Fukazawa, in *Ionic Liquids: Theory, Properties, New Approaches*, ed. by A. Kokorin, InTech, Rijeka, Croatia, **2011**, Chap. 9, pp. 201-224.
- 36 T. Sonnleitner, D. A. Turton, S. Waselikowski, J. Hunger, A. Stoppa, M. Walther, K. Wynne, R. Buchner, *J. Mol. Liq.* **2014**, *192*, 19-25.
- 37 B. R. Hyun, S. V. Dzyuba, R. A. Bartsch, E. L. Quitevis, *J. Phys. Chem. A* **2002**, *106*, 7579-7585.
- 38 J. R. Rajian, S. F. Li, R. A. Bartsch, E. L. Quitevis, *Chem. Phys. Lett.* **2004**, *393*, 372-377.
- 39 D. Xiao, J. R. Rajian, A. Cady, S. Li, R. A. Bartsch, E. L. Quitevis, *J. Phys. Chem. B* **2007**, *111*, 4669-4677.
- 40 D. Xiao, L. G. Hines, Jr., S. Li, R. A. Bartsch, E. L. Quitevis, O. Russina, A. Triolo, *J. Phys. Chem. B* **2009**, *113*, 6426-6433.
- 41 H. Shirota, A. M. Funston, J. F. Wishart, E. W. Castner, Jr., *J. Chem. Phys.* **2005**, *122*, 184512/1-12.
- 42 H. Shirota, K. Nishikawa, T. Ishida, *J. Phys. Chem. B* **2009**, *113*, 9831-9839.
- 43 H. Shirota, T. Ishida, *J. Phys. Chem. B* **2011**, *115*, 10860-10870.
- 44 H. Shirota, H. Matsuzaki, S. Ramati, J. F. Wishart, *J. Phys. Chem. B* **2015**, *119*, 9173-9187.
- 45 S. Kakinuma, S. Ramati, J. F. Wishart, H. Shirota, *J. Chem. Phys.* **2018**, *148*, 193805/1-10.
- 46 D. Xiao, J. R. Rajian, S. F. Li, R. A. Bartsch, E. L. Quitevis, *J. Phys. Chem. B* **2006**, *110*, 16174-16178.
- 47 D. Xiao, J. R. Rajian, L. G. Hines, Jr., S. Li, R. A. Bartsch, E. L. Quitevis, *J. Phys. Chem. B* **2008**, *112*, 13316-13325.
- 48 F. Bardak, D. Xiao, L. G. H. Jr., P. Son, R. A. Bartsch, E. L. Quitevis, P. Yang, G. A. Voth, *ChemPhysChem* **2012**, *13*, 1687-1700.
- 49 L. Xue, G. Tamas, R. P. Matthews, A. J. Stone, P. A. Hunt, E. L. Quitevis, R. M. Lynden-Bell, *Phys. Chem. Chem. Phys.* **2015**, *17*, 9973-9983.
- 50 E. Gurung, D. Meng, L. Xue, G. Tamas, R. M.

- Lynden-Bell, E. L. Quitevis, *Phys. Chem. Chem. Phys.* **2018**, *20*, 26558-26569.
- 51 G. Giraud, C. M. Gordon, I. R. Dunkin, K. Wynne, *J. Chem. Phys.* **2003**, *119*, 464-477.
- 52 D. A. Turton, J. Hunger, A. Stoppa, G. Hefter, A. Thoman, M. Walther, R. Buchner, K. Wynne, *J. Am. Chem. Soc.* **2009**, *131*, 11140-11146.
- 53 H. Shirota, R. Biswas, *J. Phys. Chem. B* **2012**, *116*, 13765-13773.
- 54 H. Shirota, *J. Phys. Chem. B* **2013**, *117*, 7985-7995.
- 55 H. Shirota, S. Kakinuma, Y. Itoyama, T. Umecky, T. Takamuku, *J. Phys. Chem. B* **2016**, *120*, 513-526.
- 56 R. Biswas, A. Das, H. Shirota, *J. Chem. Phys.* **2014**, *141*, 134506/1-11.
- 57 E. W. Castner, Jr., Y. J. Chang, Y. C. Chu, G. E. Walrafen, *J. Chem. Phys.* **1995**, *102*, 653-659.
- 58 C. J. Fecko, J. D. Eaves, A. Tokmakoff, *J. Chem. Phys.* **2002**, *117*, 1139-1154.
- 59 H. Shirota, S. Kakinuma, K. Takahashi, A. Tago, H. Jeong, T. Fujisawa, *Bull. Chem. Soc. Jpn.* **2016**, *89*, 1106-1128.
- 60 T. Fujisawa, K. Nishikawa, H. Shirota, *J. Chem. Phys.* **2009**, *131*, 244519-1-14.
- 61 H. Shirota, H. Fukazawa, T. Fujisawa, J. F. Wishart, *J. Phys. Chem. B* **2010**, *114*, 9400-9412.
- 62 S. Kakinuma, H. Shirota, *J. Phys. Chem. B* **2018**, *122*, 6033-6047.
- 63 S. Kakinuma, H. Shirota, *J. Phys. Chem. B* **2019**, *123*, 1307-1323.
- 64 D. A. Turton, T. Sonnleitner, A. Ortner, M. Walther, G. Hefter, K. R. Seddon, S. Stana, N. V. Plechkova, R. Buchner, K. Wynne, *Faraday Discuss.* **2012**, *154*, 145-153.
- 65 T. Sonnleitner, D. A. Turton, G. Hefter, A. Ortner, S. Waselikowski, M. Walther, K. Wynne, R. Buchner, *J. Phys. Chem. B* **2015**, *119*, 8826-8841.
- 66 J. Reichenbach, S. A. Ruddell, M. Gonzalez-Jimenez, J. Lemes, D. A. Turton, D. J. France, K. Wynne, *J. Am. Chem. Soc.* **2017**, *139*, 7160-7163.
- 67 H. Shirota, K. Takahashi, M. Ando, S. Kakinuma, *J. Chem. Eng. Data* **2019**, *64*, 4701-4707.
- 68 H. Shirota, E. W. Castner, Jr., *J. Phys. Chem. B* **2005**, *109*, 21576-21585.
- 69 T. Masaki, K. Nishikawa, H. Shirota, *J. Phys. Chem. B* **2010**, *114*, 6323-6331.
- 70 H. Shirota, T. Mandai, H. Fukazawa, T. Kato, *J. Chem. Eng. Data* **2011**, *56*, 2453-2459.
- 71 H. Shirota, *J. Chem. Phys.* **2005**, *122*, 044514/1-12.
- 72 H. Shirota, *J. Phys. Chem. A* **2011**, *115*, 14262-14275.
- 73 A. D. Becke, *J. Chem. Phys.* **1993**, *98*, 5648-5652.
- 74 C. Lee, W. Yang, R. G. Parr, *Phys. Rev. B* **1988**, *37*, 785-589.
- 75 M. J. Frisch, G. W. Trucks, H. B. Schlegel, G. E. Scuseria, M. A. Robb, J. R. Cheeseman, G. Scalmani, V. Barone, G. A. Petersson, H. Nakatsuji, X. Li, M. Caricato, A. V. Marenich, J. Bloino, B. G. Janesko, R. Gomperts, B. Mennucci, H. P. Hratchian, J. V. Ortiz, A. F. Izmaylov, J. L. Sonnenberg, D. Williams-Young, F. Ding, F. Lipparini, F. Egidi, J. Goings, B. Peng, A. Petrone, T. Henderson, D. Ranasinghe, V. G. Zakrzewski, J. Gao, N. Rega, G. Zheng, W. Liang, M. Hada, M. Ehara, K. Toyota, R. Fukuda, J. Hasegawa, M. Ishida, T. Nakajima, Y. Honda, O. Kitao, H. Nakai, T. Vreven, K. Throssell, J. J. A. Montgomery, J. E. Peralta, F. Ogliaro, M. J. Bearpark, J. J. Heyd, E. N. Brothers, K. N. Kudin, V. N. Staroverov, T. A. Keith, R. Kobayashi, J. Normand, K. Raghavachari, A. P. Rendell, J. C. Burant, S. S. Iyengar, J. Tomasi, M. Cossi, J. M. Millam, M. Klene, C. Adamo, R. Cammi, J. W. Ochterski, R. L. Martin, K. Morokuma, O. Farkas, J. B. Foresman, D. J. Fox, *Gaussian 16*. Editor, Gaussian, Inc., Wallingford, CT, **2016**.
- 76 D. A. Long, *The Raman Effect*. Editor, John Wiley & Sons, West Sussex, **2002**.
- 77 D. McMorrow, W. T. Lotshaw, *Chem. Phys. Lett.* **1990**, *174*, 85-94.
- 78 D. McMorrow, W. T. Lotshaw, *J. Phys. Chem.* **1991**, *95*, 10395-10406.
- 79 J. A. Bucaro, T. A. Litovitz, *J. Chem. Phys.* **1971**, *54*, 3846-3853.
- 80 Y. J. Chang, E. W. Castner, Jr., *J. Chem. Phys.* **1993**, *99*, 7289-7299.
- 81 J. L. McHale, *Molecular Spectroscopy*. 2nd ed., Editor, CRC Press, Boca Raton, **2017**.
- 82 S. Ryu, R. M. Stratt, *J. Phys. Chem. B* **2004**, *108*, 6782-6795.
- 83 M. D. Elola, B. M. Ladanyi, *J. Chem. Phys.* **2005**, *122*, 224506-1-15.
- 84 Z. Hu, X. Huang, H. V. R. Annapureddy, C. J. Margulis, *J. Phys. Chem. B* **2008**, *112*, 7837-7849.
- 85 T. Ishida, K. Nishikawa, H. Shirota, *J. Phys. Chem. B* **2009**, *113*, 9840-9851.
- 86 T. Ishida, H. Shirota, *J. Phys. Chem. B* **2013**, *117*, 1136-1150.
- 87 J. S. Bender, S. R. Cohen, X. He, J. T. Fourkas, B. Coasne, *J. Phys. Chem. B* **2016**, *120*, 9103-9114.
- 88 J. S. Bender, J. T. Fourkas, B. Coasne, *J. Phys. Chem. B* **2016**, *121*, 11376-11382.
- 89 S. Katsuta, Y. Shiozawa, K. Imai, Y. Kudo, Y. Takeda, *J. Chem. Eng. Data* **2010**, *55*, 1588-1593.
- 90 T. Abdallah, D. Lemordant, B. Claude-Montigny, *J. Power Sources* **2012**, *201*, 353-359.
- 91 M. L. P. Le, F. Alloin, P. Strobel, J.-C. Lepretre, C. P. d. Valle, P. Judeinstein, *J. Phys. Chem. B* **2010**, *114*, 894-903.
- 92 Z.-B. Zhou, H. Matsumoto, K. Tatsumi, *Chem.-Eur. J.* **2005**, *11*, 752-766.
- 93 D. Blanco, J. L. Viesca, M. T. Mallada, B. Ramajo, R. Gonzalez, A. H. Battez, *Surf. Coat. Technol.* **2016**, *302*, 13-21.
- 94 A. Bhattacharjee, A. Luis, J. H. Santos, J. A. P. Lopes-da-Silva, M. G. Freire, P. J. Carvalho, J. A. P. Coutinho, *Fluid Phase Equilib.* **2014**, *381*, 36-45.
- 95 K. Tsunashima, S. Kodama, M. Sugiya, Y. Kunugi, *Electrochim. Acta* **2010**, *56*, 762-766.
- 96 M. H. Ghatee, M. Bahrami, N. Khanjari, *J. Chem. Thermodyn.* **2013**, *65*, 42-52.
- 97 M. Krolikowski, M. Krolikowska, C. Wisniewski, *J. Chem. Thermodyn.* **2016**, *103*, 115-124.
- 98 O. Borodin, W. Gorecki, G. D. Smith, M. Armand, *J. Phys. Chem. B* **2010**, *114*, 6786-6798.
- 99 G. B. Appetecchi, M. Montanino, M. Carewska, M. Moreno, F. Alessandrini, S. Passerini, *Electrochim. Acta* **2011**, *56*, 1300-1307.
- 100 G. Annat, M. Forsyth, D. R. MacFarlane, *J. Phys. Chem. B* **2012**, *116*, 8251-8258.
- 101 T. Makino, M. Kanakubo, T. Umecky, A. Suzuki, T. Nishida, J. Takano, *J. Chem. Eng. Data* **2012**, *57*, 751-755.
- 102 U. Domanska, P. Okuniewska, K. Padaszynski, M. Krolikowska, M. Zawadzki, M. Wieckowski, *J. Phys. Chem. B* **2017**, *121*, 7689-7698.
- 103 G. McHale, C. Hardacre, R. Ge, N. Doy, R. W. K. Allen, J. M. MacInnes, M. R. Bown, M. I. Newton, *Anal. Chem.* **2008**, *80*, 5806-5811.
- 104 F. M. Gacino, T. Regueira, L. Lugo, M. J. P. Comunas, J. Fernandez, *J. Chem. Eng. Data* **2011**, *56*, 4984-4999.
- 105 M. Moreno, M. Montanino, M. Carewska, G. B. Appetecchi, S. Jeremias, S. Passerini, *Electrochim. Acta* **2013**,

- 99, 108-116.
- 106 U. Domanska, M. Krolikowska, K. Walczak, *J. Sol. Chem.* **2014**, *43*, 1929-1946.
- 107 V. L. Martins, A. J. R. Rennie, R. M. Torresi, P. J. Hall, *Phys. Chem. Chem. Phys.* **2017**, *19*, 16867-16874.
- 108 H. Jin, B. O'Hare, J. Dong, S. Arzhantsev, G. A. Baker, J. F. Wishart, A. J. Benesi, M. Maroncelli, *J. Phys. Chem. B* **2008**, *112*, 81-92.
- 109 J.-M. Andanson, N. Papaiconomou, P.-A. Cable, M. Traikia, I. Billard, P. Husson, *Phys. Chem. Chem. Phys.* **2017**, *19*, 28834-28840.
- 110 T.-Y. Wu, S.-G. Su, H. P. Wang, Y.-C. Lin, S.-T. Gung, M.-W. Lin, I.-W. Sun, *Electrochim. Acta* **2011**, *56*, 3209-3218.
- 111 Z.-B. Zhou, H. Matsumoto, K. Tatsumi, *Chem.-Eur. J.* **2006**, *12*, 2196-2212.
- 112 M. J. Monteiro, F. F. Camilo, M. C. C. Ribeiro, R. M. Torresi, *J. Phys. Chem. B* **2010**, *114*, 12488-12494.
- 113 K. Tsunashima, M. Sugiya, *Electrochem.* **2007**, *75*, 734-736.
- 114 F. Philippi, D. Rauber, J. Zapp, R. Hempelmann, *Phys. Chem. Chem. Phys.* **2017**, *19*, 23015-23023.
- 115 M. Hayyan, F. S. Mjalli, M. A. Hashim, I. M. A. Nashef, T. X. Mei, *J. Ind. Eng. Chem.* **2013**, *19*, 106-112.
- 116 K. R. Seddon, A. Stark, M. J. Torres, *ACS Symp. Ser.* **2002**, *819*, 34-49.
- 117 Y. Kimura, M. Fukuda, K. Suda, M. Terazima, *J. Phys. Chem. B* **2010**, *114*, 11847-11858.
- 118 R. Osada, T. Hoshino, K. Okada, Y. Ohmasa, M. Yao, *J. Chem. Phys.* **2009**, *130*, 184705/1-8.
- 119 P.-Y. Chen, C. L. Hussey, *Electrochim. Acta* **2004**, *49*, 5125-5138.
- 120 J. Sun, M. Forsyth, D. R. MacFarlane, *J. Phys. Chem. B* **1998**, *102*, 8858-8864.
- 121 A. Orita, K. Kamijima, M. Yoshida, *J. Power Sources* **2010**, *195*, 7471-7479.
- 122 H. Matsumoto, H. Sakaebe, K. Tatsumi, M. Kikuta, E. Ishiko, M. Kono, *J. Power Sources* **2006**, *160*, 1308-1313.
- 123 Y. Wang, K. Zaghbi, A. Guerfib, F. F. C. Bazito, R. M. Torresi, J. R. Dahn, *Electrochim. Acta* **2007**, *52*, 6346-6352.
- 124 C. Wolff, S. Jeong, E. Paillard, A. Balducci, S. Passerini, *J. Power Sources* **2015**, *293*, 65-70.
- 125 F. Castiglione, M. Moreno, G. Raos, A. Famulari, A. Mele, G. B. Appetecchi, S. Passerini, *J. Phys. Chem. B* **2009**, *113*, 10750-10759.
- 126 L. G. Sanchez, J. R. Espel, F. Onink, G. W. Meindersma, A. B. d. Haan, *J. Chem. Eng. Data* **2009**, *54*, 2803-2812.
- 127 S. Jeremias, M. Carewska, L. Conte, S. Passerini, G. B. Appetecchi, *RSC Adv.* **2013**, *3*, 17755-17761.
- 128 A. E. Somers, B. Khemchandani, P. C. Howlett, J. Sun, D. R. MacFarlane, M. Forsyth, *ACS Appl. Mater. Interface* **2013**, *5*, 11544-11553.
- 129 C. Yao, W. R. Pitner, J. L. Anderson, *Anal. Chem.* **2009**, *81*, 5054-5063.
- 130 U. L. Bernard, E. I. Izgorodina, D. R. MacFarlane, *J. Phys. Chem. C* **2010**, *114*, 20472-20478.
- 131 G. B. Appetecchi, M. Montanino, D. Zane, M. Carewska, F. Alessandrini, S. Passerini, *Electrochim. Acta* **2009**, *54*, 1325-1332.
- 132 Z. Chen, Y. Huo, J. Cao, L. Xu, S. Zhang, *Ind. Eng. Chem. Res.* **2016**, *55*, 11589-11596.
- 133 P. J. Fischer, M. P. Do, R. M. Reich, A. Nagasubramanian, M. Srinivasan, F. E. Kuhn, *Phys. Chem. Chem. Phys.* **2018**, *20*, 29412-29422.
- 134 H. Matsumoto, T. Matsuda, Y. Miyazaki, *Chem. Lett.* **2000**, *29*, 1430-1431.
- 135 K. Tsunashima, M. Sugiya, *Electrochem. Commun.* **2007**, *9*, 2353-2358.
- 136 D. R. Lide, *CRC Handbook of Chemistry and Physics*. 89 ed., D. R. Lide, CRC Press, Boca Raton, **2008**.
- 137 M. H. Ibrahim, M. Hayyan, M. A. Hashim, A. Hayyan, M. K. Hadj-Kali, *Fluid Phase Equilib.* **2016**, *427*, 18-26.
- 138 W. Xu, E. I. Cooper, C. A. Angell, *J. Phys. Chem. B* **2003**, *107*, 6170-6178.
- 139 H. Tokuda, K. Ishii, M. A. B. H. Susan, S. Tsuzuki, K. Hayamizu, M. Watanabe, *J. Phys. Chem. B* **2006**, *110*, 2833-2839.
- 140 H. Vogel, *Physik. Z.* **1921**, *22*, 645-646.
- 141 G. Tammann, W. Hesse, *Z. Anorg. Allg. Chem.* **1926**, *156*, 245-257.
- 142 G. S. Fulcher, *J. Am. Ceram. Soc.* **1925**, *8*, 789-794.
- 143 G. W. Scherer, *J. Am. Ceram. Soc.* **1992**, *75*, 1060-1062.
- 144 T. Iimori, T. Iwahashi, K. Kanai, K. Seki, J. Sung, D. Kim, H.-o. Hamaguchi, Y. Ouchi, *J. Phys. Chem. B* **2007**, *111*, 4860-4866.
- 145 C. Aliaga, G. A. Baker, S. Baldelli, *J. Phys. Chem. B* **2008**, *112*, 1676-1684.
- 146 L. C. Geiger, B. M. Ladanyi, *Chem. Phys. Lett.* **1989**, *159*, 413-420.
- 147 S. Kakinuma, H. Shirota, *J. Phys. Chem. B* **2015**, *119*, 4713-4727.
- 148 Y. J. Chang, E. W. Castner, Jr., *J. Phys. Chem.* **1996**, *100*, 3330-3343.
- 149 H. Fukazawa, T. Ishida, H. Shirota, *J. Phys. Chem. B* **2011**, *115*, 4621-4631.
- 150 S. Kakinuma, T. Ishida, H. Shirota, *J. Phys. Chem. B* **2017**, *121*, 250-264.
- 151 H. Shirota, T. Kato, *J. Phys. Chem. A* **2011**, *115*, 8797-8807.
- 152 A. Triolo, O. Russina, B. Fazio, G. B. Appetecchi, M. Carewska, S. Passerini, *J. Chem. Phys.* **2009**, *130*, 164521/1-6.